SANDIA REPORT

SAND97–0344 • UC–414
Unlimited Release
Printed March 1997

A Feasibility Study of Space-Charge Neutralized Ion Induction Linacs: Final Report

S.A. Slutz, P. Primm, T. Renk, D.J. Johnson, E. McGuire, T.R. Lockner, S. Humphries, Jr.

Prepared by
Sandia National Laboratories
Albuquerque, New Mexico 87185 and Livermore, California 94550
for the United States Department of Energy
under Contract DE-AC04-94AL85000.

Sandia National Laboratories

Issued by Sandia National Laboratories, operated for the United States Department of Energy by Sandia Corporation.

Available to DOE and DOE contractors from
Office of Scientific and Technical Information
P.O. Box 62
Oak Ridge, TN 37831

Prices available from (615) 576-8401, FTS 626-8401

Available to the public from
National Technical Information Service
U.S. Department of Commerce
5285 Port Royal Rd
Springfield, VA 22161

NTIS price codes
Printed copy: A04
Microfiche copy: A01

SAND97-0344
Unlimited Release
Printed March 1997

Distribution
Category UC-414

A Feasibility Study of Space-Charge Neutralized Ion Induction Linacs: Final Report

S. A. Slutz
Beam Plasma and Electromagnetic Theory Department

P. Primm, T. Renk, D. J. Johnson
Intense Beam Research Department

E. McGuire
Target Analysis and Theory Department

P. O. Box 5800 Sandia National Laboratories
Albuquerque, NM 87185-1186

T. R. Lockner
Quantum Technologies Incorporated
3701 Hawkins St. NE
Albuquerque, NM 87109

S. Humphries Jr.
University of New Mexico
Albuquerque, N.M.

Abstract

Applications for high current (> 1 kA) ion beams are increasing. They include hardening of material surfaces, transmutation of radioactive waste, cancer treatment, and possibly driving fusion reactions to create energy. The space-charge of ions limits the current that can be accelerated in a conventional ion **lin**ear **ac**celerator (linac). Furthermore, the accelerating electric field must be kept low enough to avoid the generation and acceleration of counter-streaming electrons. These limitations have resulted in ion accelerator designs that employ long beam lines and would be expensive to build. Space-charge neutralization and magnetic insulation of the acceleration gaps could substantially reduce these two limitations, but at the expense of increasing the complexity of the beam physics. We present theory and experiments to determine the degree of charge-neutralization that can be achieved in various environments found in ion accelerators. Our results suggest that, for high current applications, space-charge neutralization could be used to improve on the conventional ion accelerator technology. There are two basic magnetic field geometries that can be used to insulate the accelerating gaps, a radial field or a cusp field. We will present studies related to both of these geometries. We shall also present numerical simulations of "multicusp" accelerator that would deliver potassium ions at 400 MeV with a total beam power of approximately 40 TW. Such an accelerator could be used to drive fusion.

acknowledgments

We gratefully acknowledge many helpful discussions and encouragement from C. Olson. We thank Ingo Hofmann for suggesting that we look at plasma neutralization. We also thank D. B. Seidel, T. D. Pointon, L. P. Mix, J. W. Poukey, and S. E. Rosenthal for consultation on support for the various computer codes used in this study.

Contents

Figures

I. Introduction

A conventional induction linac involves the use of many acceleration gaps as depicted in Fig. 1

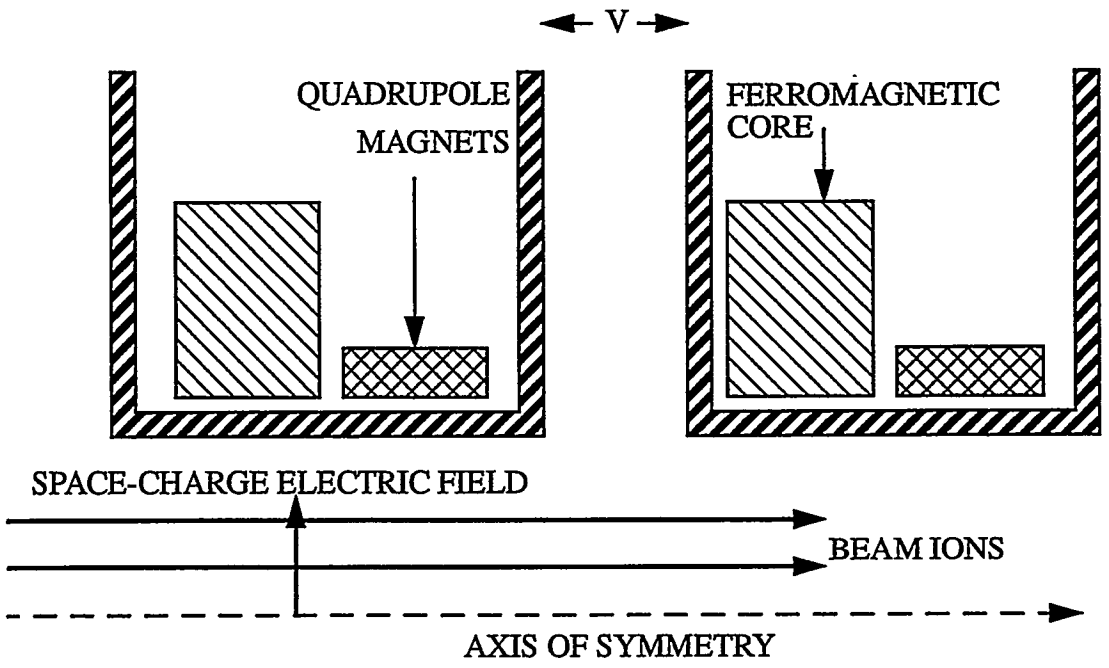

Fig. 1 A schematic of an acceleration gap for a conventional induction linac

The voltage across each acceleration gap is separated from the neighboring gaps by inductive isolation, which is enhanced by the use of ferromagnetic core materials. The integral of the voltage over time that can be applied to each gap is determined by the saturation field of the core material and the cross sectional area. The core material is a significant fraction of the cost of a conventional accelerator and thus its use should be minimized if possible. This can be accomplished by decreasing the ion pulse length and the final accelerating voltage, while increasing the ion current to maintain the beam power. However, large beam currents result in strong space-charge induced electric fields that tend to spread the ion beam outward radially. The magnitude of the electric field is given by the formula

$$E = \frac{I_B}{2\pi r \varepsilon_0 v_B} = \frac{J_B r}{2 v_B \varepsilon_0}, \qquad (1)$$

where I_B is the ion beam current, r is the radius, and v_B is the ion velocity, and J_B is the ion beam current density, MKS units will be used throughout this report. Increasing the beam radius decreases the outward electric field, but it also increases the mass (cost) of the core material. The ion beam is held together by the use of quadrupole magnets, with an alternating gradient direction. The amount of current that can be transported is then determined by the strength of the quadrupole focussing magnets. This limit could be increased if the space-charge of the ion beam is partially cancelled by the presence of electrons, which have the opposite charge. We refer to this as space-charge-neutralization. These electrons could be introduced into the beam from the drift tube walls or possibly by the injection of some plasma into the beam path. However, electrons within the vicinity of the acceleration gaps will be accelerated in the direction opposite of the ions. Since electrons are much lighter than ions they will obtain higher velocities than the ions and will constitute an undesirable loss of power. This loss can be avoided by applying a strong magnetic field across the accelerating gap. Single particle equations of motion indicate that the electrons will not be able to cross the gap when the following condition is satisfied

$$\Psi_A - \Psi_C > \frac{r_A mc}{e}\sqrt{\left(1+\frac{eV}{mc^2}\right)^2 - 1}, \qquad (2)$$

where $\Psi = rA_\theta$ is the magnetic stream-function with the subscripts (a,c) for points on the anode and cathode, m/e is the mass-to-charge ratio of an electron, V is the voltage across the gap, and c is the speed of light. An electron leaving the cathode is turned back toward the cathode before reaching the anode as long as this relationship is satisfied. Equality of both sides of relation (2) defines maximum magnetic insulation voltage, V_c.

It has been demonstrated that accelerating field strengths considerably in excess of the breakdown threshold can be used efficiently when the accelerating gap is magnetically insulated[1], which is an added advantage of using magnetic insulation. The possibility of significantly reducing the length of an ion induction linac by using magnetic insulation

and space-charge neutralization has been recognized for quite some time[2]. Experiments were conducted with several acceleration stages insulated by a radial magnetic field[3], see Fig. 2

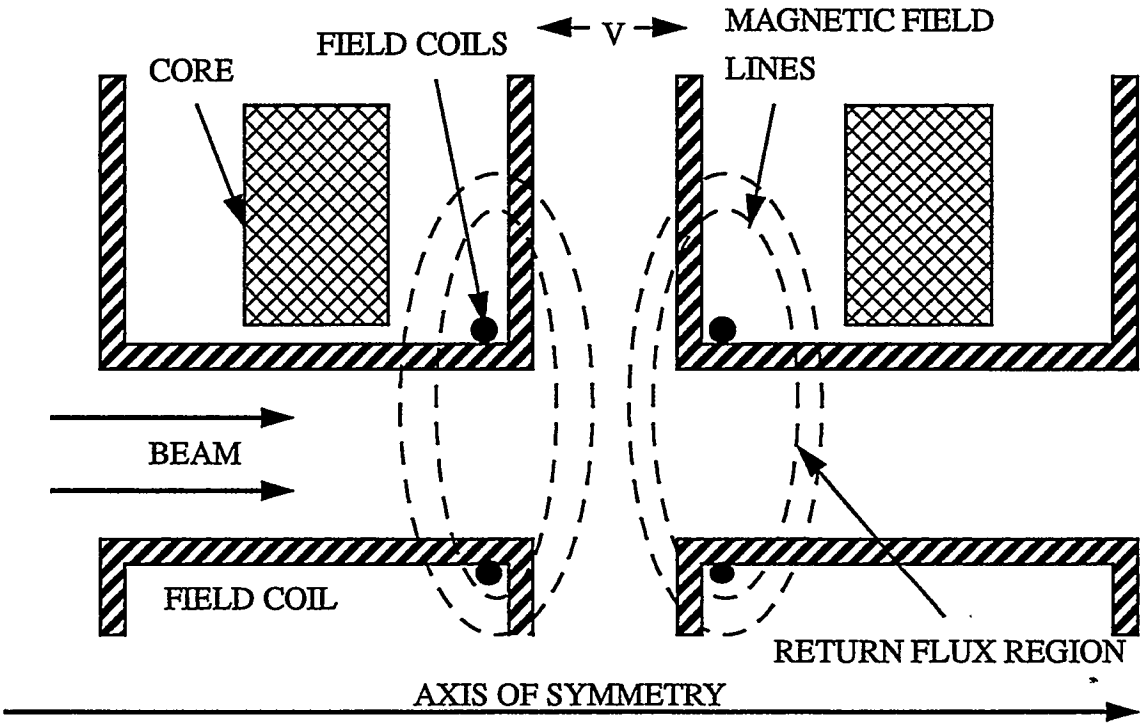

Fig. 2 Schematic of an accelerator gap using a radial magnetic field for insulation.

Efficient insulation and post acceleration was demonstrated, but several problems were also found. The charge neutralization in the return flux region was not sufficient for efficient transport between stages. Successful operation necessitated a gas background, which is incompatible with acceleration in a constant ion charge state. Furthermore, the inner field coils needed to generate a radial magnetic field, required support structures (not shown in the figure) that blocked a portion of the annular beam. Repetitive operation of such an accelerator would cause severe erosion of these supports and would produce outgassing that could result in beam stripping. Finally, the azimuthal symmetry of the beam was removed by the support structures. This caused inefficiencies in the accelerating gaps and could result in beam emittance growth. We shall address some of these issues in this report. We shall show that a sufficiently high degree of charge-neutralization can be

obtained by using a preformed plasma and that the ions will not be stripped for a reasonably short accelerator. However, achieving the required beam intensity with only a few acceleration stages implies large diamagnetic forces on the applied magnetic field, which will result in focussing of the beam at each acceleration stage. We will present an analytic calculation to determine the magnitude of this effect.

Using only field coils outside of the beam results in a cusp field[4,5] to insulate the accelerating gaps. This *multicusp* geometry does not require a central conductor, which greatly simplifies the construction, see Fig. 3. The bulk of our work was directed toward studying the feasibility of this field geometry,

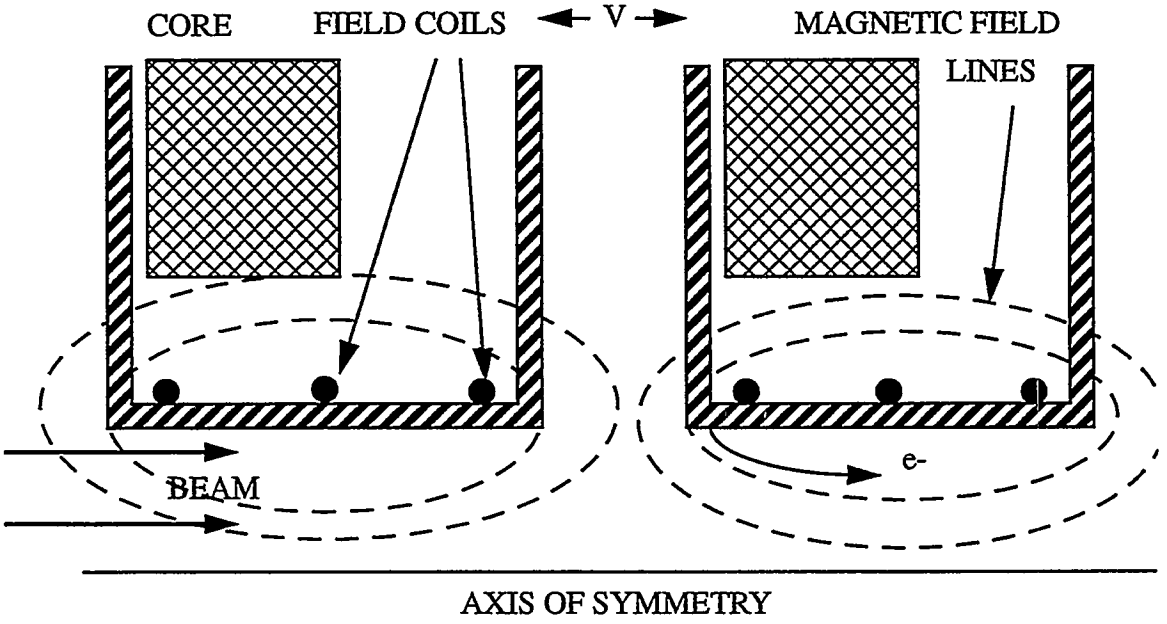

Fig. 3 A schematic of an acceleration stage of a multicusp accelerator.

The ion beam entering from the left is accelerated by a voltage V at the gap, which is insulated by a cusp magnetic field. Notice how the cusp geometry allows electrons to enter and follow the beam to the next acceleration stage. As the beam ions enter the drift region, they are forced to rotate azimuthally as they cross the cusp field. This rotation leads to a focussing force (solenoidal focussing) in the drift region that is proportional to the square of the magnetic field strength. The maximum current density, which can be transported in

the drift region can be found by balancing the net space-charge force against the solenoidal focussing force. The result is

$$J_{SX} = \frac{eZ\varepsilon_0\beta cB^2}{2M(1-f)}, \tag{3}$$

where eZ/M is the charge to mass ratio of the ion, βc is velocity of the ion, B is the strength of the magnetic field, and f is the degree of space-charge neutralization. The critical parameter is the degree of space-charge neutralization. Notice that the current density scales as e/M, so this type of accelerator scheme will be more effective for lower mass ions and thus would be very effective at accelerating protons. Such an accelerator could be used to generate neutrons, which can be used for a variety of applications. Medium mass ions such as potassium would be more appropriate for a fusion driver, so that high beam intensities can be reached with the proper range of the ion in the ICF capsule.

II. Focussing constraints on ion induction linacs for inertial fusion

The DOE-sponsored program to develop high-intensity accelerators as inertial fusion drivers has been active for about two decades. As envisioned, an induction linac generates multiple beams of 10 GeV uranium ions with a 10 ns pulse length. The beams propagate ballistically to a small target in a reactor chamber. The accelerator and its attendant beam transport lines are complex and occupy a considerable amount of space. Over the span of the Heavy Ion Fusion program, technical problems that involve conventional accelerator theory (such as the design of achromatic final focussing lens with ideal space-charge forces) have been pursued with vigor. In contrast, several daunting problems reflecting the unprecedented beam intensity levels have not been emphasized. Advanced concepts (such as beam neutralization and self-pinched propagation) have been consistently portrayed as potential solutions but not seriously addressed. In principal, the space-charge neutralization methods developed at Sandia National Laboratories for the Light Ion Fusion program

could impact the design of a fusion accelerator. Neutralization would allow higher current transport. Therefore, the required total energy could be generated by beams with reduced kinetic energy and ion mass.

The goal of this report is to quantify whether neutralization can significantly impact accelerator driven fusion. The long duration of the Heavy Ion Fusion program testifies that the determination of feasibility is not a straightforward issue. We shall derive simple constraints on the allowable focussing errors for two test cases: a heavy-ion fusion accelerator generating unneutralized beams of uranium at 10 GeV (β=.3), and an intermediate-mass accelerator that utilizes beam neutralization to accelerate potassium ions (A=39) to 400 MeV (β=.15). The target proposed for heavy ions is optimized for the rather long range of heavy ion accelerators and requires a focal spot of 1-3 mm. The significantly shorter range of light ions has the allowed the development of a spherically irradiated target that requires a focal spot of approximately 1 cm. Our medium mass ion would have a range comparable to light ions (~20 mg/cm^2) and could drive a light ion target. The acceptable angular divergence at the final focussing lens of the accelerator depends on the focal spot and the focal length through the simple formula

$$\Delta\Theta = \frac{r_f}{L}, \tag{4}$$

where L is the focal length, and r_f is the focal spot size. Heavy ion studies assuming ballistic transport from the final focussing lens to the target require L to be as large as 10 m. Light ion studies with neutralized ballistic transport have assume L~2 m. If self-pinch propagation works the focal length could be made much smaller, less than a meter for light ions. The maximal transverse energy spread (temperature) at the final lens is given by

$$\delta T = (\Delta\Theta)^2 T_0, \tag{5}$$

where T_0 is the final ion kinetic energy. For the ballistically focussing heavy ion case, the allowed transverse temperature is 100-900 eV (depending on the focal size). For the

medium mass ion the maximal transverse temperature is approximately 10-40 KeV (depending on the range of L=1-2m). Clearly transverse temperature can be much larger for the medium mass case, because of the larger focal size and shorter focal length.

Next, consider possible sources of transverse beam energy. A low value of δT implies that there is a close balance on average between applied focusing forces and the force of beam generated electric field. The standard heavy ion approach is based on the transport of bare beams. The space charge potential of the beam is given by the expression

$$\Phi_B = \frac{I_B}{4\pi\varepsilon_0 v_B}. \tag{6}$$

The pulse length on the target must be less than 10 ns, but the pulse length could be as long as 100 ns at the final focussing lens if beam bunching is used. Assuming 20 beams the current in each beam must be 250 A to put 500 TW on target. Thus the beam potential is approximately 25 KeV, which is much larger than the maximum transverse temperature. The maintenance of the low beam transverse temperature requires linear focusing focussing forces and an almost perfectly uniform beam. Consider the contrasting approach of neutralized beam transport. Since collective neutralization is not an easily controllable process, there is little hope of obtaining a partially neutralized beam where the residual field is linear. Therefore the goal is to keep the residual fields low as possible. Assuming 20 beams and a bunching factor of 3 due to the shorter focal length, the medium mass driver must have approximately 20 kA/beam. The beam potential is thus about 4 MV. This potential must be reduced by a combination of charge-neutralization and focussing forces. Assuming the charge-neutralization reduces the beam space-charge potential by the factor, α, the focussing force must produce a negative potential greater than $\alpha\Phi_B$ to contain the beam. Let's assume that this containment factor is $1+\beta$, then $\alpha\beta\Phi_B$ must be less than maximum allowed transverse temperature or $\alpha\beta < 0.01$. In the next section we shall present simulations of the charge-neutralization process, which indicate that $\alpha \cong 0.04$.

This implies that $\beta < 0.25$ will be required. Designing a focussing system with this degree of accuracy does not seem impossible, but may prove to be difficult due to the nonlinearity of the net space-charge forces. In the next section we shall show that a preformed plasma could produce very high degrees of neutralization so that $\alpha < 0.01$. Another possibility is that the accelerator is short enough so that ions do not have sufficient time to obtain a transverse temperature equal to the beam potential. Consider the distance ions travel as they perform one transverse oscillation

$$\Delta z > 2\pi v_B r_b \sqrt{\frac{2\pi M v_b \varepsilon_0}{\alpha\beta e I_B}}, \tag{7}$$

which is about 125 m for our medium mass example. The degree of nonlinearity determines how many of these oscillations are necessary before the ion transverse energy is randomized. This will depend on the specific accelerator scheme, but in general it should be easier to obtain a high quality beam if the accelerator is not very long. Thus light to medium mass accelerators are probably the most promising.

III. Theory of space-charge neutralization

A. Vacuum

i. No magnetic field

The space-charge neutralization process in a vacuum is conceptually quite simple, but is very difficult to treat analytically. As the head of an ion beam passes a region of drift tube wall, an electric field is generated by the space-charge of the beam. If this field is large enough the drift tube wall undergoes electrical breakdown and becomes a source of electrons. As an example, eq. (3) gives a maximum current density J=11 A/cm^2 for a potassium beam at $\beta = 0.13$, assuming a solenoidal field strength of 5 Tesla and f=0.1. Without neutralization the electric field at the edge of a 20 cm beam according to eq. (1) would be 350 KV/cm, which is more than sufficient to cause electrical breakdown at the

drift tube wall. Note that it may be advantageous to provide a source of electrons such as a thermionic emitter to avoid any time delay introduced by the breakdown process. Electrons are then pulled into the beam from the wall. A simple analytic estimate of the neutralization provided by these electrons was made by Stuhlinger[6]. He assumed that a constant density beam arrived instantaneously and then electrons were allowed to fall into the potential well caused by the ion space-charge. His result indicated a neutralization factor of approximately 0.5. The low neutralization factor calculated analytically is because all of the electrons are forced to have zero total energy. Thus the electrons have a maximum velocity at the center of the beam and zero velocity at the drift tube walls. Hence the electron density profile does not match the ion density profile. In fact, the electrons will not all have the same energy, due to the finite risetime of the beam current density. This spread in the electron energies results in much better neutralization than the simple analytic model predicts. Numerical techniques provide the most straightforward way to find solutions for the self consistent motion of the electrons emitted from the drift tube walls in response to the electric field generated by the unneutralized portion of the ion space-charge.

We have studied this process numerically using the 3-D particle-in-cell (PIC) code QUICKSILVER[7,8]. QUICKSILVER performs a fully dynamic solution to Maxwell's equations with relativistic three-dimensional particle kinematics and the full Lorentz force. To solve Maxwell's equations, the volume of interest is divided into discrete cells, and electric and magnetic fields are associated with each cell. Discrete particles, each representing 10^9-10^{12} electrons or ions, are used to simulate the electron and ion flow and provide a self-consistent source for the field solutions. The relativistic equations of motion are solved for each particle in the electromagnetic field. Electrons and ions are introduced into the system by emission from the electrode surfaces. The charge of each particle is determined by assuming space-charge-limited emission and enforcing Gauss' Law for cells immediately adjacent to the electrodes. Similarly, particles encountering metal

boundaries are removed from the system. Voltage boundary conditions can be specified that introduce electromagnetic energy into the simulation. It should be kept in mind, that due to computer storage limitations, the number of simulation particles is less than 10^6 and consequently the numerical solutions will probably underestimate the degree of charge neutralization.

Consider an unneutralized ion beam propagating between two parallel plates separated by a distance 2H. The space-charge limited current density is found by equating the space-charge potential at the midplane to the energy of the ions. The result is

$$J_{SC} = 2\varepsilon_0 \sqrt{\frac{2eZ}{M}} \frac{W^{3/2}}{H^2}, \tag{8}$$

where W is the energy of the ions.

To study beam neutralization, we set up the simple simulation geometry shown in Fig. 4

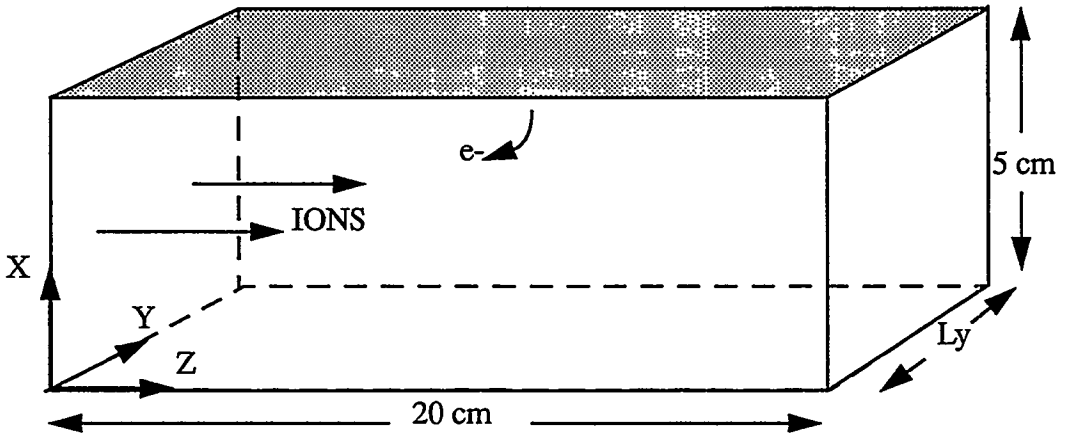

Fig. 4 Simulation geometry to study the basic vacuum neutralization process. The boundary conditions are periodic at y=0 and y=L_y. Mirror symmetry is assumed at x=0. All other surfaces are conducting. Ions are injected through the surface at z=0. Electrons are only emitted from the shaded surface.

The edges of the simulation at y=0 and y=L_y are connected by periodic boundary conditions, i.e. a particle exiting through one of these surface comes back into the simulation

from the other surface. The distance L_y was varied from 1 cm to 5 cm with negligible changes in the degree of neutralization. Mirror symmetry is assumed about the plane x=0. All surfaces are conducting and electrons are only emitted from the shaded surface. A proton beam (1 MeV) is injected through the z=0 surface and exits through the opposite surface. We set J=5A/cm^2, which is $J_{SC}/2$ and ran simulations with and without electrons for comparison. The beam potential at x=0 and z=10 cm is defined by $\int_0^H E dx$, where H=5 cm is the half height of the box. This potential is shown for both of these simulations in Fig. 5.

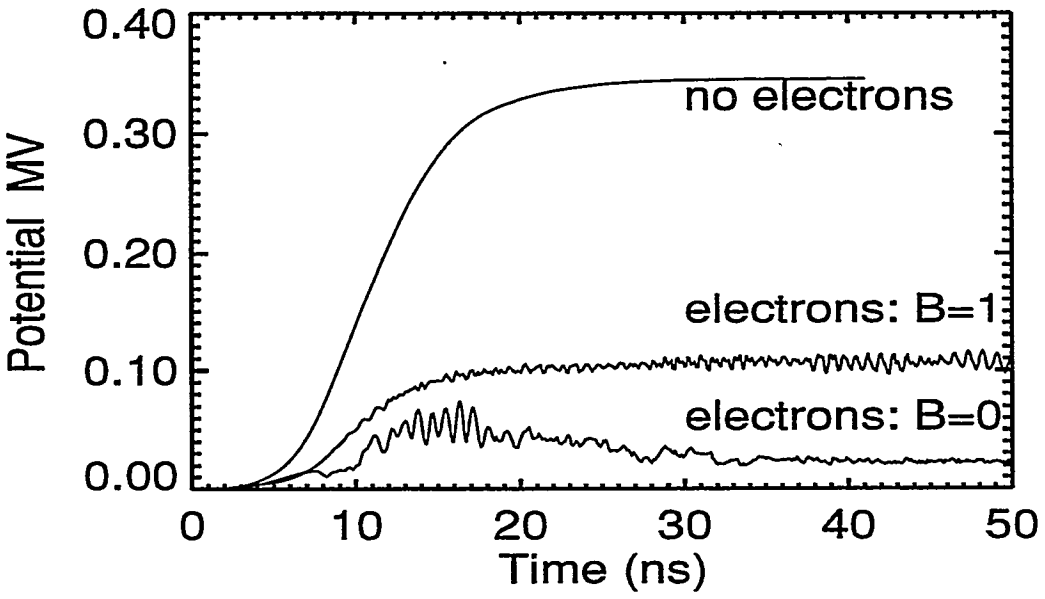

Fig. 5 The electric potential at the simulation midplane is plotted for three different simulations, a) without neutralizing electrons, b) with electrons and a 1 Tesla magnetic field in the x-direction, and c) electrons but no magnetic field.

The result without electrons is slightly less than 500 KeV due to the spreading of the beam and loss to the drift tube walls. Allowing electron emission reduces the potential by more than a factor of 10 when no magnetic field is present. Late in time, the degree of neutralization is approximately 0.96.

ii. The effect of magnetic fields.

The magnetic field in the return flux region of a radially insulated acceleration gap is primarily transverse to the direction of ion propagation. Electrons will be free to enter the beam from the drift tube walls, but will not be able to follow the beam, thus charge-neutralization will be possible, but not current neutralization. The results of a simulation with a 1 Tesla field in the x-direction are shown in Fig. 5. The neutralization is roughly 80%, which is considerably worse than for the B=0 case. This behavior explains the poor transport than was observed on the Pulselac experiments.[3]

We ran several simulations of ion beams injected across an acceleration gap insulated by a cusp magnetic field. Since a cylindrical coordinate system cannot be used in QUICKSILVER for a simulation that includes r=0, we used Cartesian geometry as in the previous simulations. The cusp magnetic field was calculated using the magnetic field solving code ATHETA[9]. We found that electrons remained tied to the magnetic field lines, even though electromagnetic fluctuations developed in the simulation, see Fig. 6. A proton beam is injected at a velocity of c/10 and current density, $J=J_{SX}\sim 26$ A/cm^2 as determined by Eq. (3) assuming a neutralization factor of 0.9. The periodic length, L_y, was 10 cm, which was sufficient to allow electromagnetic fluctuations to develop through instabilities such as the diocotron[10]. The magnetic field lines are also plotted and it is apparent that the electrons do not migrate across the magnetic field. This is in distinct contrast, to the behavior of simulations of light ion diodes, which exhibit significant electron migration across the magnetic field lines[10]. The difference in the behaviors of these two systems can be explained by the following argument. In the absence of electromagnetic fluctuations the electrons move in electromagnetic fields that are independent of time and the y-coordinate. Thus from Hamilton's equations, the energy and y-component of the canonical momentum are conserved. The electron motion consists of cyclotron orbits superimposed on an average drift in the **E x B** direction. Instabilities generate fluctuations that have vari-

ations in both time and the y-coordinate and thus the energy and canonical momentum of the electrons is not strictly conserved.

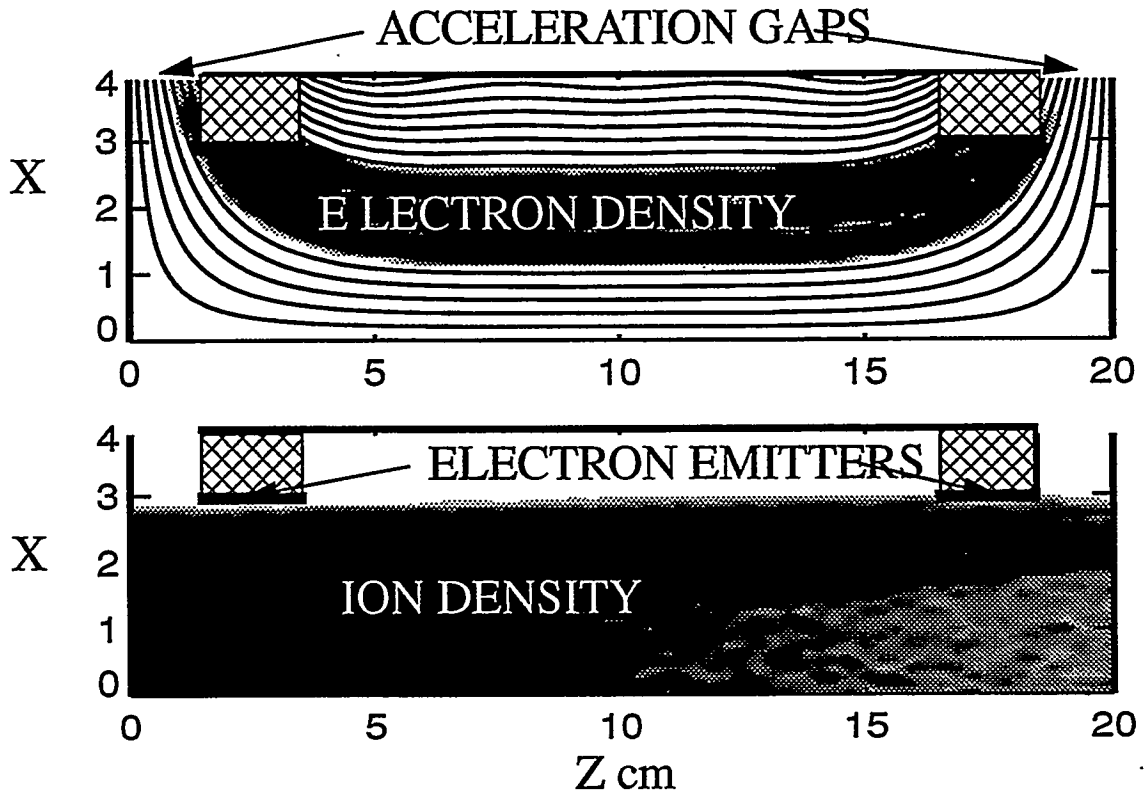

Fig. 6 Grey scale contours of the electron and ion densities from simulations of a proton beam injected into a cusp field are plotted. The magnetic field lines are shown in the top figure. Ions are injected from the z=0 surface, while electrons are emitted from the upper surfaces at x=3 cm.

However, from Chaos theory we know that a sufficiently small perturbation of an integrable system will not produce diffusion over the dynamical phase-space. The magnitude of the fluctuations is approximately two orders of magnitude larger in the light ion diode simulations than for our present simulations. Apparently the fluctuation amplitude for the present simulations is too small to generate chaotic electron motion. Note that electrons are not emitted from within the accelerating gap, since they would be able to cross the gap upstream and form a counter-streaming electron beam that would significantly reduce the efficiency of the accelerator. Thus the central (near the midplane in our cartesian simulation) of the beam is not space-charge neutralized. The ion beam charge density is also

shown in Fig. 6 (bottom). We have made a detailed comparison of the ion and electron density for $r > r_i$ (r_i is the inner radius of the electron cloud), which indicates approximately 90% space-charge neutralization. The space-charge induced electric field for $r < r_i$, exerts a force larger than the inward solenoidal force; thus, this portion of the beam expands. This can be seen in Fig. 7, which is a phase space plot of ions exiting the simulation.

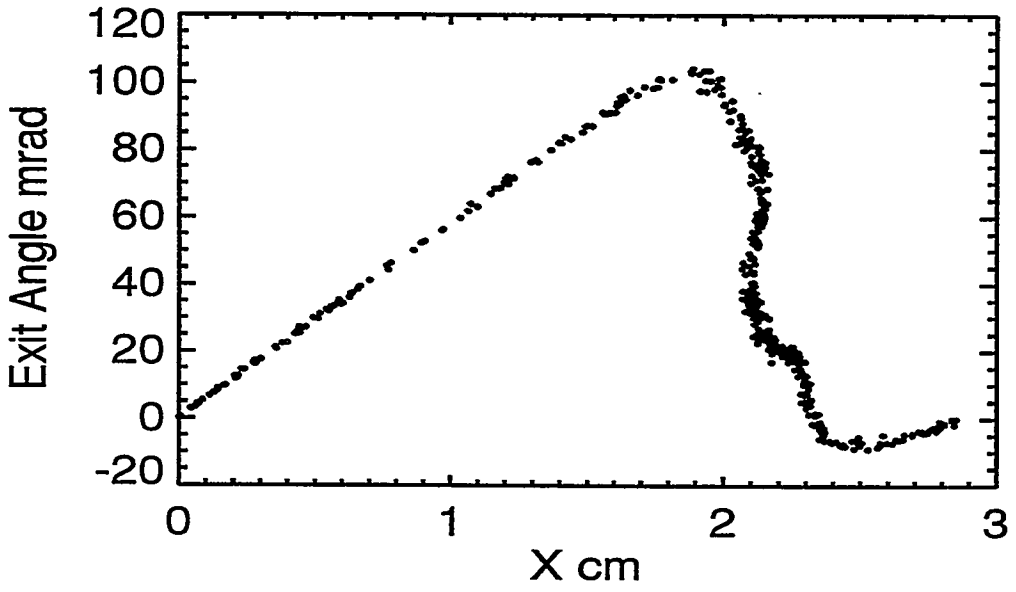

Fig. 7 Plot of the ion exit angle as a function of x.

A laminar equilibrium could be set up by injecting two different beam densities determined by eq. (3) with f=0 for $r < r_i$ and f~0.9 for $r > r_i$. However, any finite transverse beam temperature will cause these two beam regions to mix with a resulting increase in transverse temperature or emittance. A model of this process will be presented in section VI.

B. Preformed plasma for space-charge neutralization

We will show that a background plasma can provide sufficient space-charge neutralization of an ion beam to allow propagation for several tens of meters without significant stripping of the ions. The plasma density needs to be larger than the beam density, but as we will show it does not have to be very much larger. The net charge of the plasma is zero and thus when the beam enters the plasma the plasma-beam ensemble will still have a net charge. However, the electrons in the plasma will be displaced inward to cancel the extra positive space-charge of the beam. The much less mobile plasma ions will remain approximately in their original position and a positive sheath will develop at the edge of the plasma. The electric field outside of the plasma sheath will be as large as it would have been without the plasma, but the beam will be effectively screened from its own electric field as we shall show with the following analytic models and numerical simulations.

i. Spatially homogenous finite amplitude model of plasma neutralization

In this model we assume a cylindrically symmetric beam of infinite radius and axial extent. The beam density is given as a function of only time. We ignore the motion of the plasma ions and only follow the radial motion of the electrons. Since the problem is spatially homogeneous the radial position of each electron is given by the product its initial radial position and a function of time, thus $r = r_0 h(t)$. Poisson's equation and Newton's law then lead to a second order differential equation for h(t) given by

$$\frac{d^2 h}{d\tau^2} + (1 + g(\tau)\Delta)\frac{h}{2} = \frac{1}{2h} \tag{9}$$

where $\tau=\omega_p t$, ω_p is plasma frequency at the initial density, Δ is the maximum beam density normalized to the plasma density and $g(\tau)$ is the time dependence of the beam density. The ratio of beam potential with and without the plasma is then given by

$$\frac{\phi}{\phi_0} = g(\tau) + \frac{(h^2 - 1)}{\Delta h^2}. \tag{10}$$

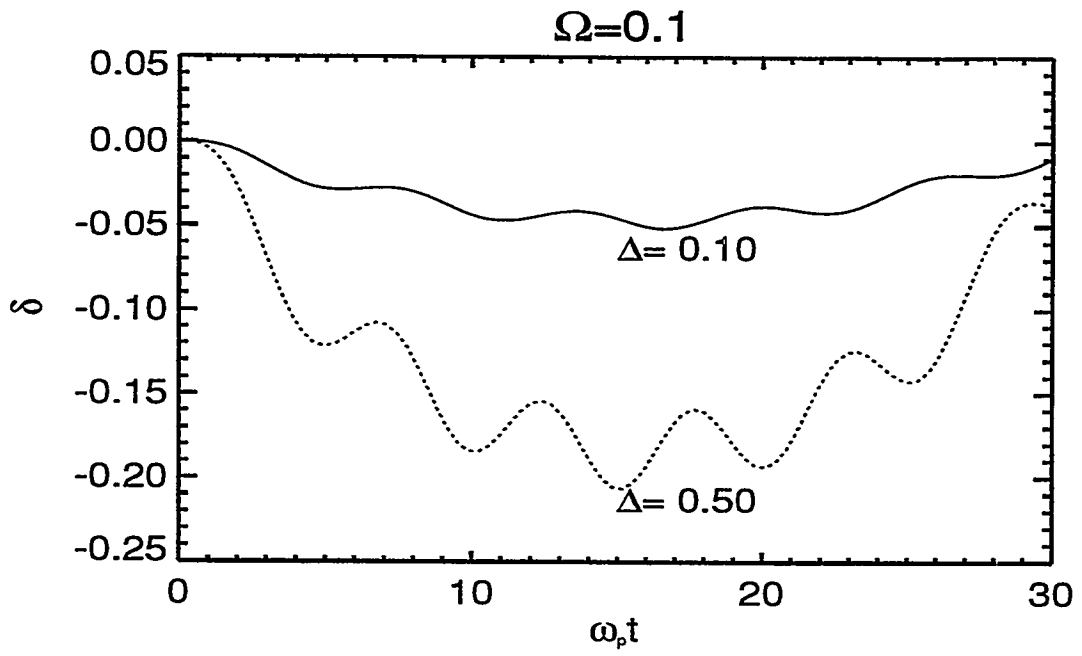

Fig. 8 The time dependent position of the electrons

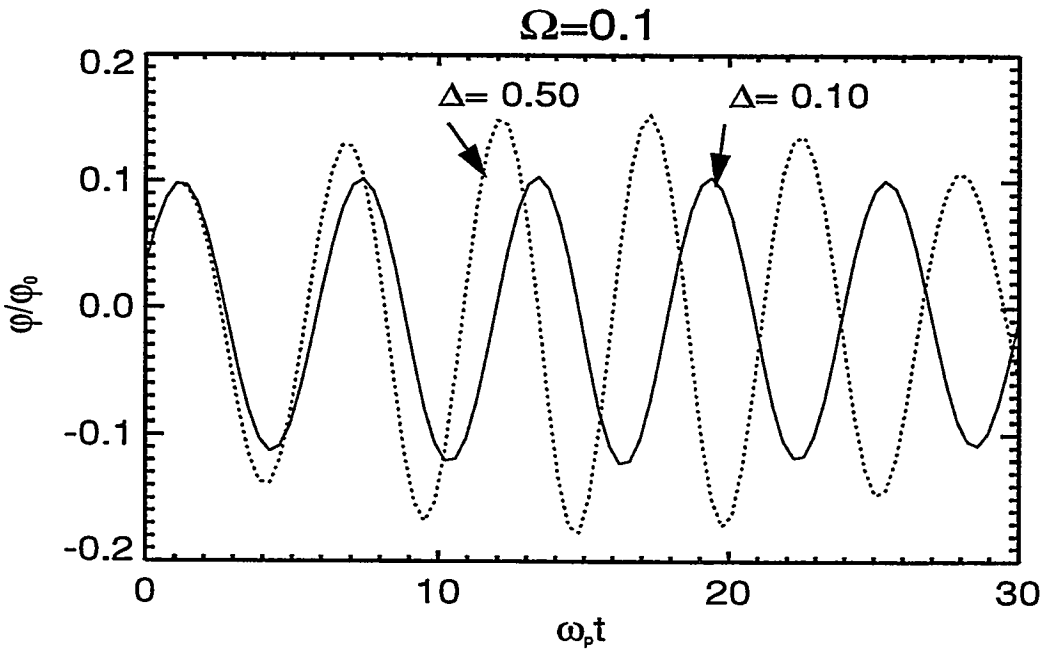

Fig. 9 The normalized beam potential as a function of time.

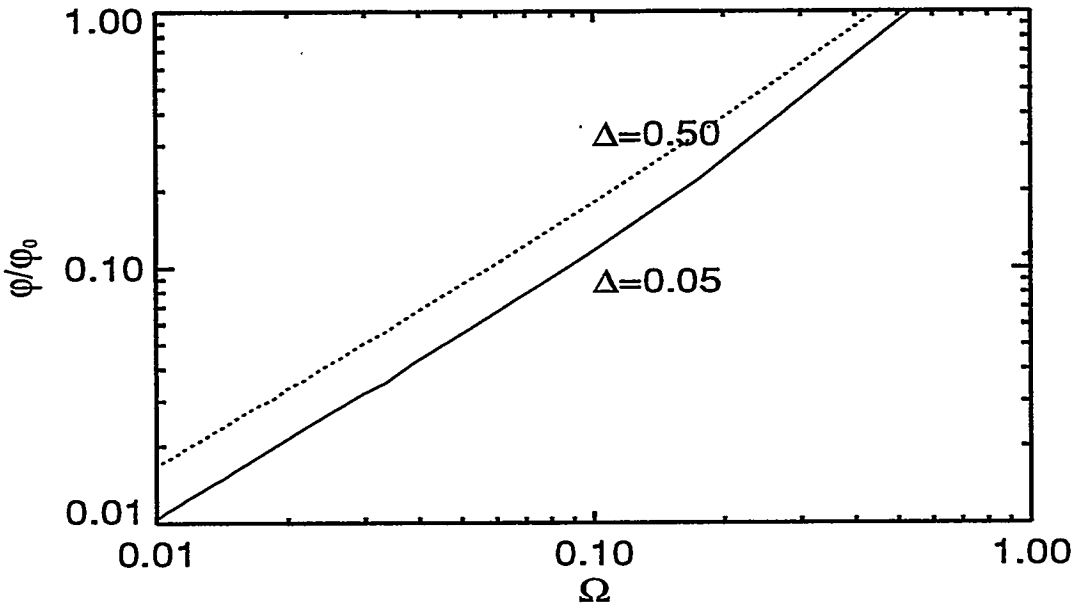

Fig. 10 The normalized potential is plotted as a function of Ω

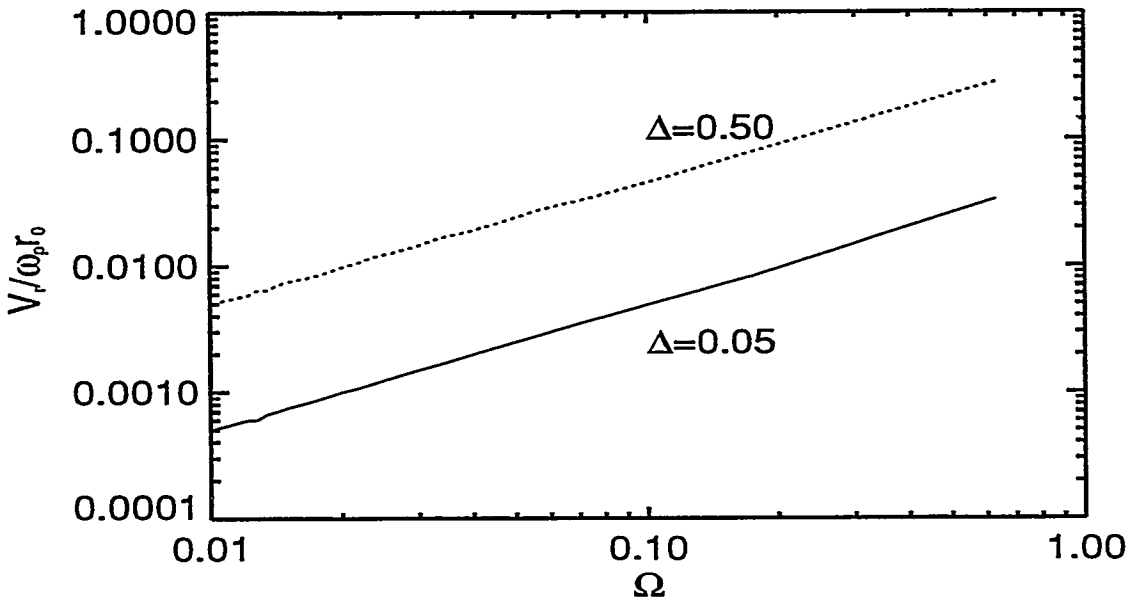

Fig. 11 The normalized electron velocity is plotted as a function of Ω

A convenient choice of $g(\tau)$ is $\sin(\Omega\tau)$, where $\Omega = \frac{\pi}{\omega_p t_p}$ and t_p is the ion pulse length. We have integrated eq. (9) for different values of Δ and Ω. The displacement of the electrons from their initial position, $\delta = \frac{r - r_0}{r_0}$ is shown in Fig. 8. As expected, the plasma electrons move less and the neutralization is better as the plasma density is increased. Fig. 9 shows the time dependent potential ratio given by eq (10). The maximum ratio of $\frac{\Phi}{\Phi_0}$ is plotted as a function of Ω in Fig. 10. The normalized electron velocity is plotted as a function of Ω in Fig. 11.

Analytic results can be obtained for small values δ and Δ. Eq. (9) then becomes

$$\frac{d^2\delta}{d\tau^2} + \delta = -\frac{\Delta g(\tau)}{2} \tag{11}$$

which for our choice of $f(\tau)$ has the solution

$$\delta = \frac{\Delta}{2(1-\Omega^2)}(\Omega\sin\tau - \sin\Omega\tau). \tag{12}$$

Substitution of eq (12) into eq (10) yields $\frac{\phi}{\phi_0} = \Omega\sin\tau$. Thus the potential fluctuates at the plasma frequency with an amplitude given by $\Omega = \frac{\pi}{\omega_p t_p}$. This result agrees well with the Δ=0.05 curve of Fig. 10 and surprisingly well with the Δ=0.5 curve. Clearly the plasma has to be only a factor of two denser than the beam to effectively space-charge neutralize the beam.

ii. Spatially inhomogeneous infinitesimal amplitude

In this model we allow the beam to have a spatial variation in the direction of propagation given by the expression

$$\rho_b = \Delta\rho_p \sin(\Omega\Lambda)\Theta(\Lambda), \tag{13}$$

where $\Lambda = \tau - \frac{\omega_p z}{v_i}$ and the theta function is zero for $\Lambda<0$ and unity for $\Lambda>0$. Linearizing the continuity and momentum equations and substituting into Poisson's equation we obtain the differential equation

$$\frac{d^2\rho}{d\Lambda^2} + \rho = \Delta \sin\Omega\Lambda\Theta(\Lambda), \tag{14}$$

where ρ is the variation in the electron density. This can be solved by the method of Laplace transforms noting that $\rho(\Lambda = 0) = \dot{\rho}(\Lambda = 0) = 0$. The result is

$$\rho(\Lambda) = \frac{\Delta}{1-\Omega^2}(\sin\Omega\tau - \Omega\sin\tau) \tag{15}$$

At the peak density of each ion pulse this yields $\frac{\rho_T}{\rho_b} = \frac{\phi}{\phi_0} \cong \Omega$ for small values of Ω. This is the same result that we obtained from the previous model.

The plasma density needs to be only several times the beam density. The ion current density in a light ion fusion accelerator is approximately 1 kA/cm^2 with a beam velocity of (2-4)x10^7 m/s and a pulse length of 10-20 ns. Thus the ion density is~ (1.5-3)x10^{12} cm^{-3} and Ω is less than 0.004. The results of these two models of plasma neutralization implies a degree of neutralization better than 99.6%. The beam density is less in a heavy ion accelerator. Thus a lower density plasma could be used. This has the advantage that the beam could propagate further before stripping would be a problem, but the degree of neutralization would not be as high.

iii. Warm electron Boltzmann distribution

The previous two models dealt with the electrons as a cold fluid solving only for the collective oscillatory motion. However, we expect the electrons to be heated by instabilities. In particular ions are streaming through the plasma, which will drive the two-stream instability. We expect the instability to saturate when the electron thermal velocity is comparable to the ion streaming velocity, v_b, i.e. $kT = \frac{mv_b^2}{2}$. We have constructed a simple planar model of the electron density profile by assuming that $\rho_e = \rho_0 e^{\frac{e\phi}{kT}}$ and the ions remain essentially immobile. Assuming cartesian geometry to simplify the calculations, Poisson's equation can be put into the dimensionless form

$$\frac{1}{2}\frac{d^2\Psi}{d\xi^2} = \rho_0 e^{\Psi} - \rho_i, \tag{16}$$

where densities are normalized to the initial plasma density, $\Psi = \frac{e\phi}{kT}$, $\xi = \frac{x}{\lambda}$, and λ is an effective Debye length defined by,

$$\lambda = \frac{v_b}{\omega_p} \tag{17}$$

Equation (16) can be integrated once analytically. We performed the second integral numerically.

We find that at the edge of the plasma the electric field is the same as if the plasma were not there, but the field decays exponentially within the plasma. The scale length is the Debye length as one would expect. There is also an electric field at the edge of the beam when the Debye length is comparable to the beam half thickness (radius in cylindrical geometry, see Fig. 12.

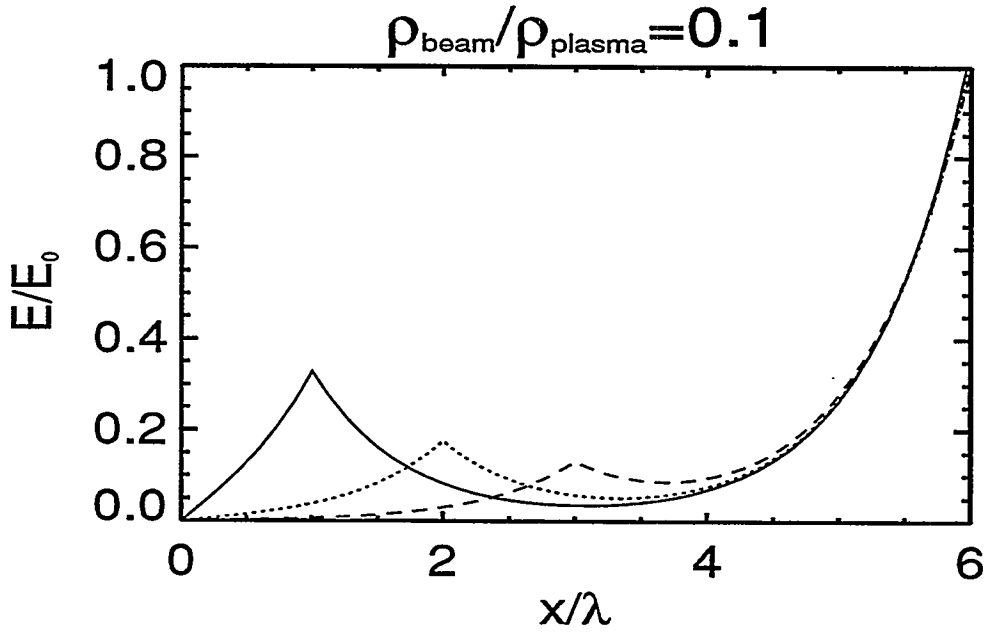

Fig. 12 The electric field calculated from equation (16) for three different beam radii normalized to the Debye length, r_b/λ=1,2, and 3, r_p/λ=6. Note the inflection occurs at the beam radius.

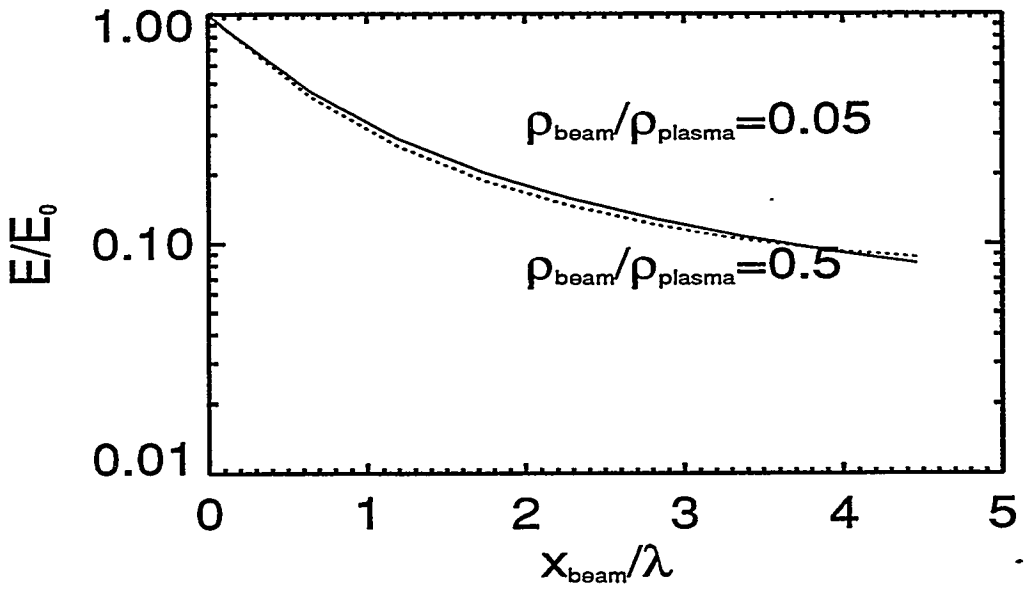

Fig. 13 The normalized electric field as a function of the normalized beam radius for two different values of the beam to plasma density.

The model predicts good space-charge neutralization as long as the Debye length is small compared to the beam radius as seen in Fig. 13. In practice this is not a problem for heavy or light ion applications.

iv. Particle-in-cell simulations

We performed simulations using the two-dimensional particle-in-cell (PIC) code, MAGIC[9]. The numerical technique used in this code is essentially the same as our previous description of QUICKSILVER. As an example, particles representing the protons and electrons of a hydrogen plasma, with a density of 6.25×10^{12} cm^{-3}, were initially loaded into the simulation region, which had conducting boundaries at r=2mm and z=0 and z=2 cm. A Bismuth beam of radius 1 mm was injected at a velocity of 9.4e7 m/s and a current density of 3.25 kA/cm^2. According to eq. (17) the Debye length should be approximately 0.7 mm. However, the electrons did not heat up to a thermal temperature comparable to the ion velocity and consequently the neutralization is better than would be indicated by

the results of the last section. The resulting radial electric field is shown in Fig. 14. The unneutralized electric field would be approximately 20 MV/m

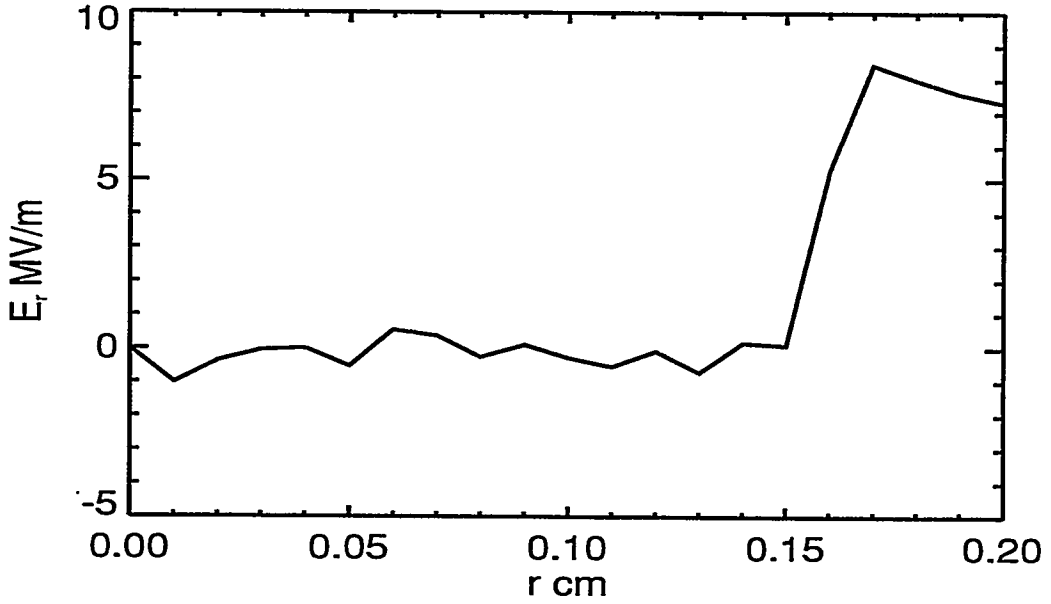

Fig. 14 The electric field as a function of radius for a simulation of a Bismuth beam injected into a hydrogen plasma

v. Ion stripping

Typical light ion beam current densities are approximately 1 kA/cm^2, which at a beam velocity of 3.e7 m/s, corresponds to a particle density of 2x10^{12} cm^{-3}. Therefore a plasma density of 1x10^{13} cm^{-3} should be more than sufficient. We have estimated the electron impact ionization of the beam ions using the formulas of Lotz[11]. The results indicate the beam should travel more than 100 m before ionization. We have calculated the ionization cross section of hydrogen and carbon ions using the plane wave Born approximation[12]. We chose lithium to represent light ion fusion applications. The results are shown in Fig. 15. We chose gold as an example of a heavy ion, see Fig. 16. The cross section decreases with ionization state, due to the loss of electrons.

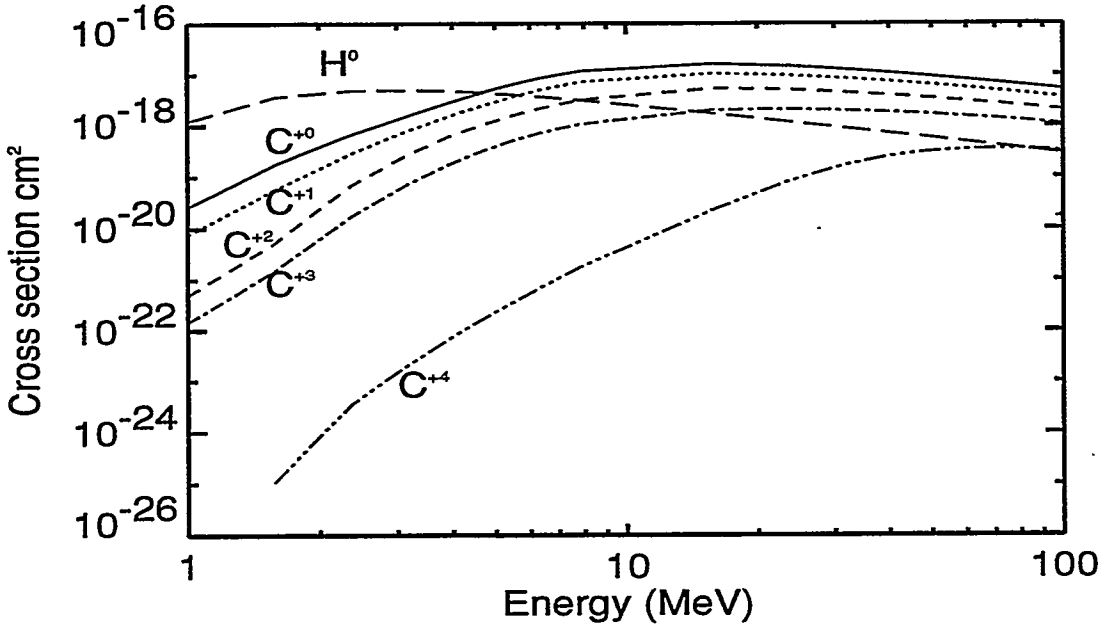

Fig. 15 The ionization cross section for Li^+ on various ions (beam energy~30 MV).

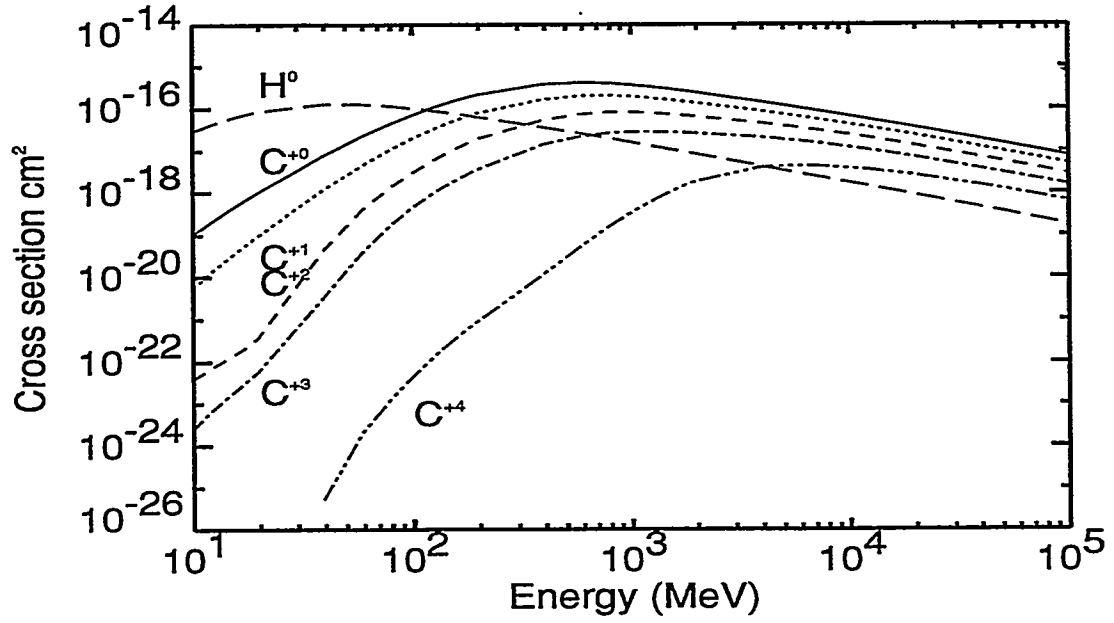

Fig. 16 The ionization cross section for Au^+ on various ions (beam energy~5GeV).

Examination of Fig. 15 indicates that the ionization cross section should be less than $1x10^{-17}$ cm^2 for a carbon plasma and less than $1x10^{-18}$ cm^2 for a hydrogen plasma. Therefore, a lithium ion should be able to travel approximately 100 m in a carbon plasma and up to a kilometer in a hydrogen plasma. The cross sections are about the same for a 1 GeV gold ion and typically the beam particle density is lower, so these beams could travel even further without significant ionization.

IV. Experimental determination of the degree of space-charge neutralization

A. Experimental facility and diagnostics

The space-charge neutralization experiments were performed using the Advanced Light Ion Accelerator System (ALIAS). The system consists of a 10 ohm, 1 MV water blumlein, which drives two transmission lines feeding power to a magnetically insulated ion diode. The configuration of the diode is shown in Fig. 17

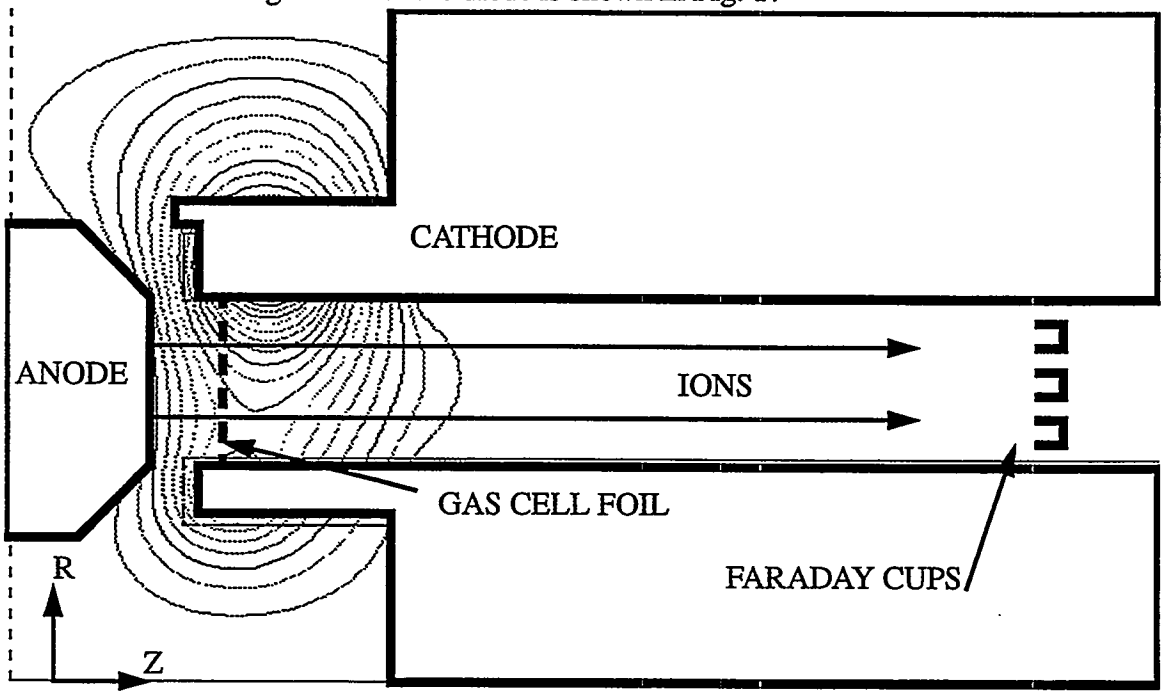

Fig. 17 Alias diode configuration

A flashover ion source, felt polishing pad, was used with a flux excluding anode. Flashover ion sources yield roughly 50% protons. The rest of the ions are dominated by various ionization states of carbon. The peak voltage at the diode was approximately 500 kV yielding proton current densities of roughly 50 A/cm^2. The anode emitting region was from r=5.2-7.8 cm for an area of about 100 cm^2. The mylar gas cell foil was nominally 2 μm thick. We used an unconventional type of Faraday cup, which we call *solid state F-cups*, which were constructed from coaxial cable. Mylar foil was placed between the end of the coaxial cable and an end-cap with a hole, see Fig. 18. The film provided electrical insulation so these cups did not require a vacuum as conventional cups do. The foil is thin enough so that protons can penetrate and be collected on the central conductor of the coaxial cable. However, this foil plus the gas cell foil would stop carbon ions or other impurity ions.

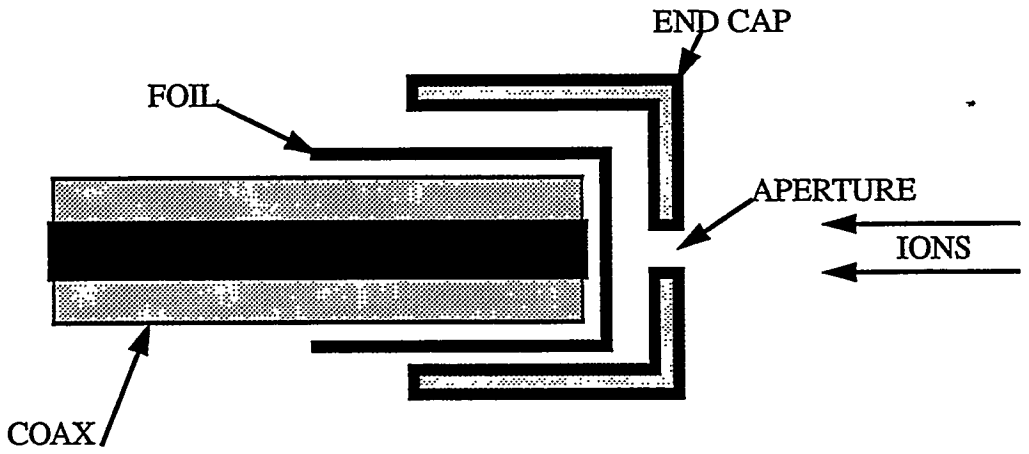

Fig. 18 Schematic of the solid state F-cup

The heating from the ions will vaporized the film and consequently increase the electrical conductivity. We estimate that the shunt resistance provided by the vaporized mylar should be about 900 Ω based on formulas for the conductivity of mylar induced by electron beams[13]. We tested this by comparing biased and unbiased cups. The results were

consistent with our estimate and indicated that we might be underestimating the ion current by about 15%, which is smaller than the shot to shot variation in the ion current density. The F-cup measurements were made at a variety of radial and azimuthal locations, to determine the transport of the ion beam

B. Results and discussion

We conducted three basic experiments. In the first set of shots we measured to ion current density at a position 25 cm down stream from the anode. These measurements were made with gas (500 mTorr) in the gas cell to provide charge-neutralization and without gas.

We compared the ratio of the current densities obtained to determine the degree of space-charge neutralization that was achieved without the gas, by assuming that the ion trajectories were essentially ballistic when the gas is present. This is not an unreasonable assumption since there is a large body of data indicating nearly perfect space-charge neutralization in gas. The experimental geometry is cylindrical but the radial thickness of the beam is small compared to the mean radius of the beam so we shall use cartesian geometry (x corresponds to radius and y corresponds to azimuth) to analyze the blow up of the beam due to space-charge. The envelope equation for a beam expanding due to its own space-charge can be calculated by making the usual paraxial approximation and assuming the beam current density is uniform at any axial location. The result is

$$\frac{d^2x}{dz^2} = \Gamma, \tag{18}$$

where $\Gamma = \frac{\alpha e J_0 x_0}{\varepsilon_0 M v_B^3}$, $\alpha = 1 - f$ is the unneutralized fraction of the beam charge, J is the beam current density, x is the beam thickness, e/M is the charge to mass ratio of the ion, v_B is the ion velocity, and the subscript 0 refers to quantities at the anode. Equation (18) can be integrated twice to yield

$$\frac{x}{x_0} = \frac{\Gamma z^2}{2} + z\left(\frac{dx}{dz}\right)_0 + 1 \tag{19}$$

In the first series of experiments we did not have a measurement of the initial divergence of the beam near the anode $\left(\frac{dx}{dz}\right)_0$, so we assumed it was zero. Thus the ion current density measured with gas was assumed to be roughly the same as at the anode. This was in reasonable agreement with Faraday cup measurement taken near the anode. The decrease in the current density due to space-charge beam blow up could then be used to infer the degree of space-charge neutralization that was achieved in vacuum. We then calculate the degree of space-charge neutralization from the equation

$$f = 1 - \frac{2\varepsilon_0 M v_B^3}{eJ_{gas}z^2}\left(\frac{J_{gas}}{J_{vac}} - 1\right) \tag{20}$$

where z=25 cm was the transport distance to the F-cups. Our results were consistent with an average neutralization of 98% in vacuum, somewhat better than indicated by the numerical simulations of section III. Moving the drift tube walls away from the beam resulted in a noticeable reduction in the degree of neutralization

In the second series of experiments we attempted to measure the space-charge neutralization in the region of the applied magnetic field. This is the region that has been of the most concern to accelerators such as Pulselac. The approach was to aperture the beam at two distances from the anode and detect the expanding beam at three different locations for each of the apertures. The basic geometry is shown in Fig. 19. The apertures were located at two different azimuthal quadrants at 3 and 6 cm from the anode. The aperture was centered radially in the beam with a width of 1 cm. Radiachromic film was placed at 1 cm intervals from each of the apertures. Each piece of film was displaced azimuthally from the next to avoid shadowing. The radiachromic film turns blue when exposed to ionizing radiation such as a proton beam. We scanned and digitized the film to determine the beam width at each film location.

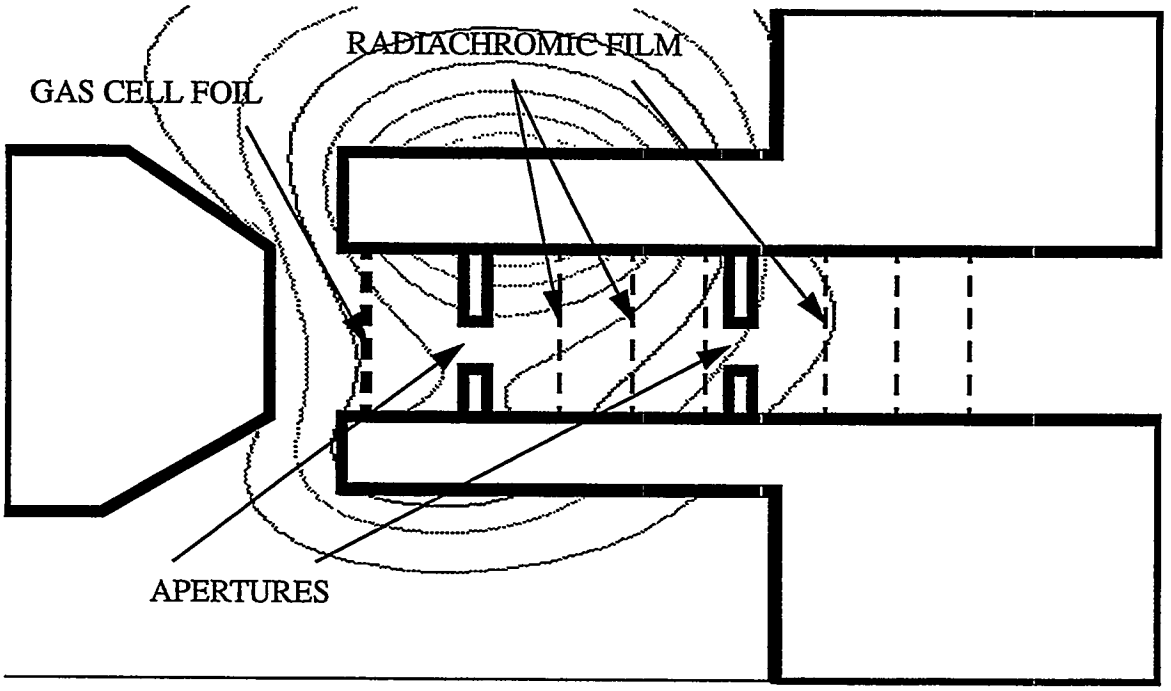

Fig. 19 Schematic of the experimental configuration to measure the space-charge neutralization in the applied field region

We took a series of seven diode shots with 500 mTorr of air pressure in the gas cell and with no air (vacuum). The results are shown in Fig. 20. Clearly the beam transport is better with the 500 mTorr of air. It should be noted that the beam was blowing up pretty badly before it entered the first aperture. This was probably due to the felt anode, which is convenient to field, but does not produce a high quality beam. We used the envelope equation (19) to determine the charge-neutralization by performing a least square fit to this experimental data. The best fit indicated a charge-neutralization of 93% for the gas fill and 83% for the vacuum shots. The value of 83% for vacuum transport in the presence of an applied field is very close to what we would expect from the simulations presented in section III. We were somewhat surprised that the gas transport was not better. The low neutralization may be due to the low ion current density (50 A/cm^2) as compared to most light ion experiments where the current density exceed 1 kA/cm^2. Thus although the gas density is 1.5×10^{16} cm^{-3}, the plasma density could be much lower.

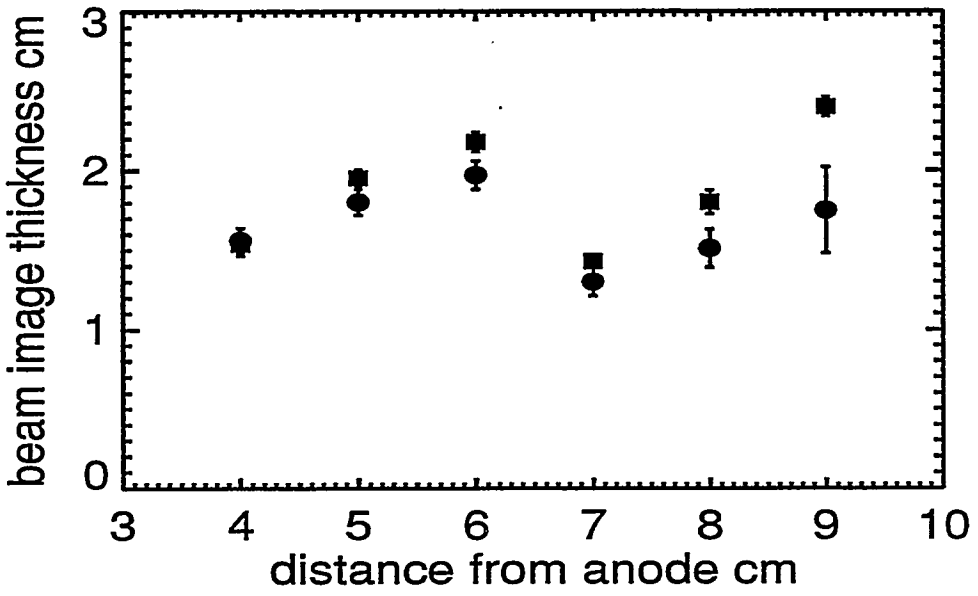

Fig. 20 The measured thickness of the beam as a function of radiachromic film location. One cm apertures are located at 3 and 6 cm. The squares are for vacuum transport, the circles are for 500 mTorr of air. The error bars are one standard deviation calculated from the shot to shot variation.

We fabricated carbon spark gaps to pre-fill the drift region of the diode with plasma. The spark gaps were nominally 1 mm and were coated with a carbon based aerosol. Six gaps were driven in series at a spacing of 1 cm along a strip line oriented in the axial direction. Twenty four of these strip lines were arranged azimuthally around the diode on the inner beam drift tube wall as depicted in Fig. 21. We tested the output of one of the spark gaps by using probes with two grids. The first grid was biased negative to stop electrons. The voltage on the second grid was varied over positive potentials to stop a portion of the ions. From this data we were able to determine that roughly 60% of the ions were C^{+4}, 20% were protons and the rest dominated by various ionization states of carbon. We also were able to measure the plasma flux and estimate that a plasma density greater than $1x10^{13}$ cm^{-3} should be produced at 1-2 cm from the gaps.

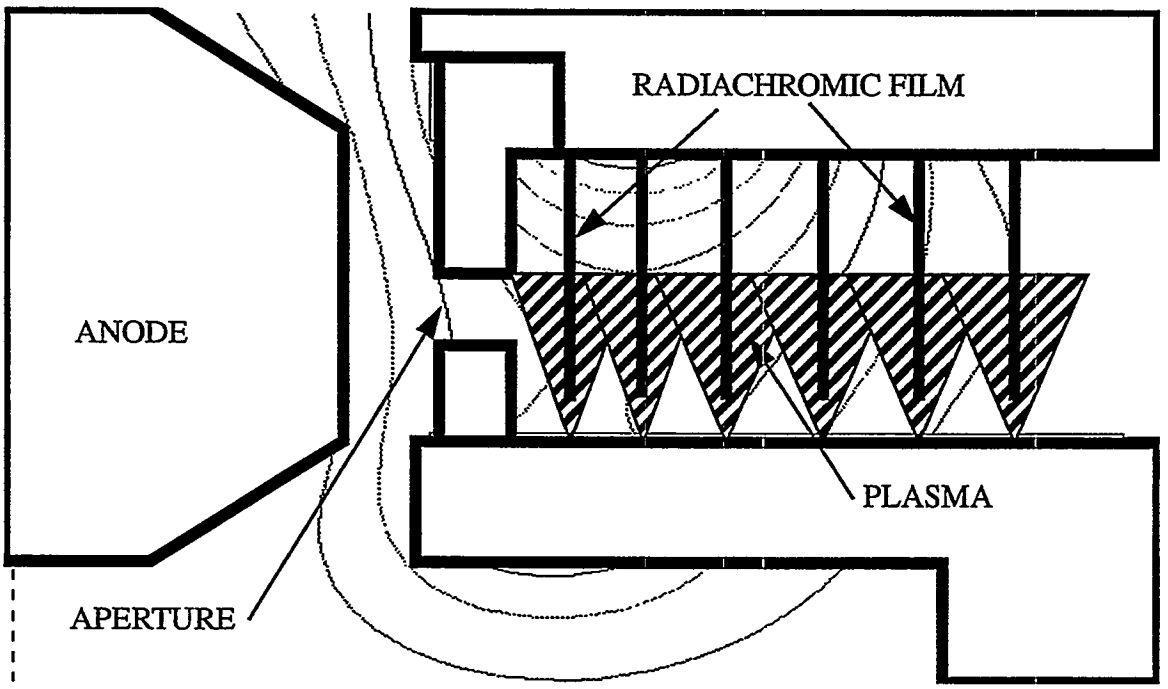

Fig. 21 Schematic of the plasma injection experiments

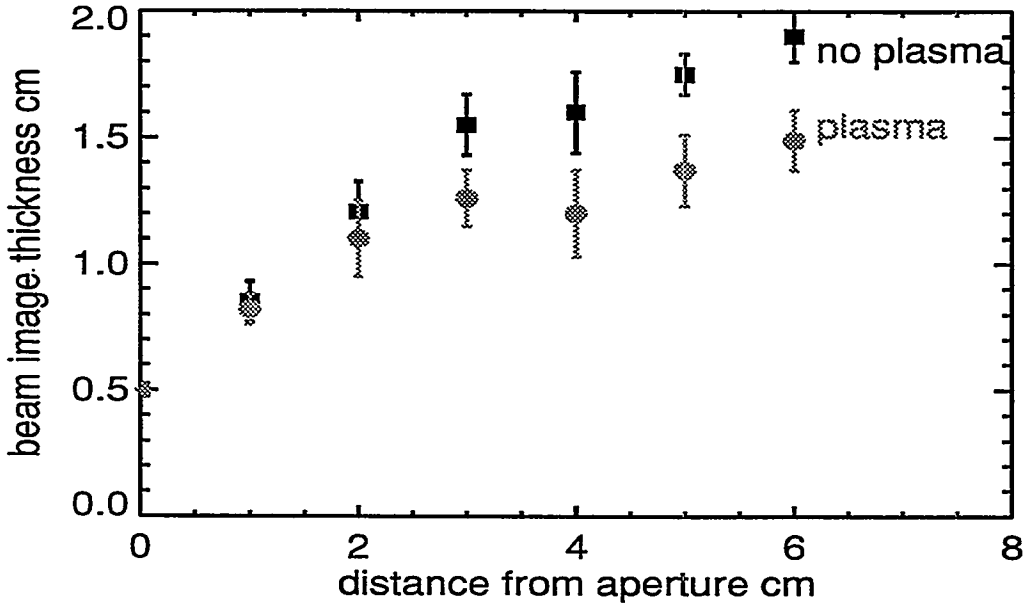

Fig. 22 Beam image at various radiachromic film locations for shots with and without plasma.

The gaps were spaced at 1 cm so that the plasma from each spark should overlap with the adjacent spark at the position of the apertured beam. In fact, it was clear from the images on the radiachromic film that the overlap was barely adequate and most of the time the plasma was pretty nonuniform over the transport region of the beam. Despite the crudeness of our set up, the data indicates that the transport was improved by plasma injection. Fig. 22 shows the results of 10 shots without plasma and 11 shots with plasma. The beam expansion is less with the plasma injection.

V. Radial magnetic field linac

A. Introduction

In the last two sections we presented theory and experiments on the degree of space-charge neutralization that can be obtained in vacuum and in plasmas. We found that 96% neutralization was obtainable in vacuum as long as no magnetic field is present. However, a magnetic field of only 1 Tesla significantly reduced the degree of neutralization even when the magnetic field was normal to the surface emitting the electrons. The neutralization is negligible if the magnetic field is tangent to the emitting surface. This result explains the poor transport that was observed in the return flux region of the radially insulated pulselac experiments. Our results on plasma neutralization indicate that this problem could be solved by injecting plasma into this region. We will now address another potential problem.

The acceleration of ions in a magnetically insulated gap must be balanced by an equal and opposite force on the electrodes. Since the electric field can be nearly zero at both the anode and the cathode, due to space-charge-limited emission at these surfaces, most of this force is delivered to the electrodes through the magnetic field. In a single-stage ion diode the force is primarily delivered to the anode by a local increase in the magnetic field on the anode side of the virtual-cathode. This increase in the anode magnetic field is

caused by the displacement of the virtual-cathode flux surface toward the anode by the JxB force of electrons within the sheath. The virtual-cathode flux surface is squashed up against the anode and assumes the approximate shape of the anode. This behavior allows one the control the focussing of the diode by shaping the anode surface. However, in a multi-stage diode there may be no surface to squash the virtual-cathode flux surface against. Consequently, the magnetic flux surfaces can become significantly bowed and this could cause excessive beam focussing. One could place a grid or a foil on the up-stream or down-stream side of each acceleration gap to control the shape of the virtual-cathode, but clearly this adds significant complexity to a multi-stage accelerator. Furthermore, both a grid and a foil would add divergence to the beam and a foil would strip the ions. We present analytic calculations of the distortion of the virtual-cathode flux surface. The results indicate that magnitude of the distortion may be acceptable for a two-stage diode with beam parameters suitable for driving fusion. Increasing the number of stages will further decrease the bending of the virtual-cathode.

B. Calculations

We assume a Cartesian geometry to as shown in Fig. 23 to simplify the calculations. This is a reasonable approximation since $\Delta r << r$. An initial magnetic field, B_0, is applied in the z-direction. The ion beam is incident from the left and is accelerated across the gap by a voltage V_2. A virtual-cathode is formed along the flux surface attached to the down stream electrode. The deformation of this flux surface is shown schematically. The electric potential is constant along the virtual-cathode and so the ions are focussed. We shall assume that the electron sheath is very thin (the super-insulated model). The problem can then be divided into two regions. Upstream from the virtual-cathode (region 1) and downstream from the virtual-cathode (region 2). We shall ignore the electric current of the ion beam in this calculation and thus Amperes law then reduces to Laplace's equation in both regions.

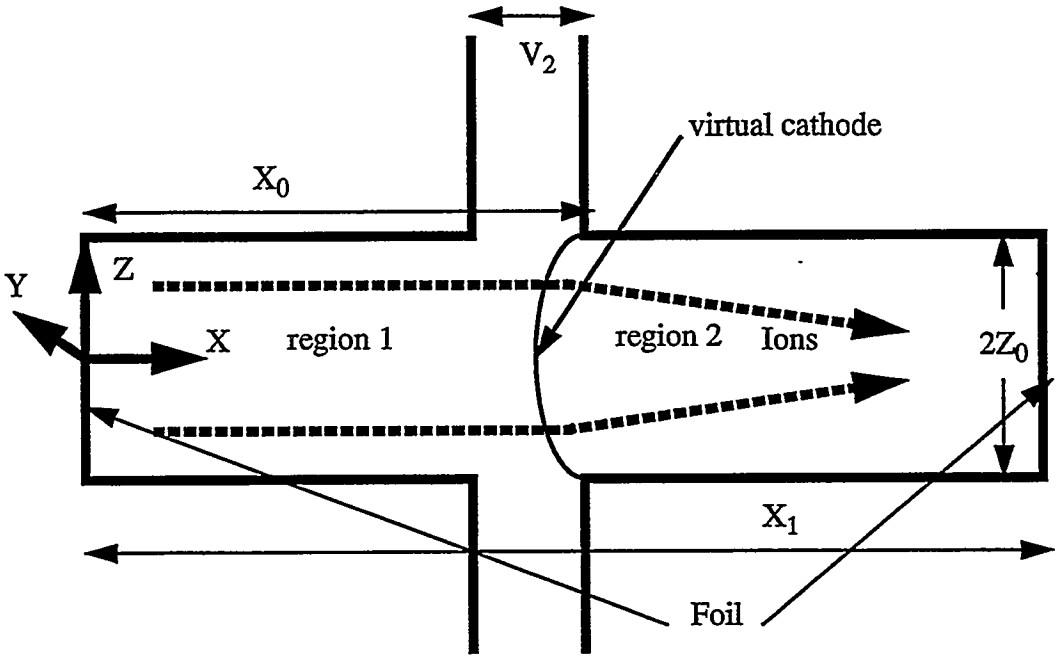

Fig. 23 Schematic of an acceleration gap with a virtual cathode

Thus we have the separable equation

$$\nabla^2 A_y = \frac{\partial^2 A_y}{\partial x^2} + \frac{\partial^2 A_y}{\partial y^2} = 0, \qquad (21)$$

where A_y is the vector potential in the y-direction. The vector potential can be divided into two components, $A_y = B_0 x + A$ where the first term is due to the applied magnetic field and the second term is due to electron sheath current in the virtual-cathode. We assume that on the beam acceleration time scale the drift walls are essentially perfect conductors and thus A=0 at these surfaces. We have shown foils (or grids) at x=0 and $x=x_1$ in Fig. 23 to represent the possible location of a foil or a grid. Thus we set A=0 for $|z| = z_0$, x=0, and $x=x_1$. Note, that there is no wall at $|z|=z_0$, within the acceleration gap. We have ignored this, which should be a good approximation as long as the gap is small compared to $2z_0$. Thus we obtain

$$A_1 = \sum_n A_{1n} \sinh(\alpha_n x) \cos(\alpha_n z) \tag{22}$$

$$A_2 = \sum_n A_{2n} e^{-\alpha_n x} \sinh[\alpha_n (x - x_1)] \cos(\alpha_n z) \tag{23}$$

where $\alpha_n = \left(n + \frac{1}{2}\right)\frac{\pi}{z_0}$. Let the position of the virtual cathode be x_0-δx, where

$$\delta x = \sum_n X_n \cos \alpha_n z. \tag{24}$$

Keeping first order quantities we obtain

$$A_{1n} \sinh(\alpha_n x_0) = A_{2n} e^{-\alpha_n x} \sinh(\alpha_n (x_0 - x_1)) \text{ and} \tag{25}$$

$$X_n = \frac{A_{1n}}{B_0} \sinh(\alpha_n x_0) \tag{26}$$

Since we have assumed that the electron sheath is thin, the magnetic force exerted on the virtual-cathode is due to the jump in magnetic pressure across the sheath, that is

$$\Delta\left(\frac{B^2}{2\mu_0}\right) = P_b = J\sqrt{\frac{2M}{Q}}\left(\sqrt{V_1 + V_2} - \sqrt{V_1}\right), \tag{27}$$

where V_1 is the effective voltage of the ion entering the acceleration gap.

If we assume $B_{z1} = B_0 + \frac{\Delta B}{2}$ and $B_{z2} = B_0 - \frac{\Delta B}{2}$, we obtain $\Delta B_z = \frac{\mu_0 P_b}{B_0}$, where $B_z = \frac{dA}{dx}$. Using this jump condition we can find the coefficients A_{1n}, A_{2n}, and X_n. The result is

$$A_{1n} = -B_0 z_0 R_p D_n \frac{\sinh \alpha_n (x_0 - x_1)}{\sinh \alpha_n x_1}, \tag{28}$$

$$A_{2n} = -B_0 z_0 R_p D_n \frac{e^{\alpha_n x_1} \sinh \alpha_n x_0}{\sinh \alpha_n x_1}, \text{ and} \tag{29}$$

$$X_n = -z_0 R_p D_n \frac{\sinh \alpha_n x_0 \sinh \alpha_n (x_0 - x_1)}{\sinh \alpha_n x_1}. \tag{30}$$

where $R_p = \frac{2\mu_0 P_b}{B_0^2}$ and $D_n = \frac{(-1)^n}{\left[\left(n+\frac{1}{2}\right)\pi\right]^2}$. The deflection of the virtual-cathode at the midplane of the beam (z=0) is maximized by letting x_0 and x_1-x_0 go to infinity. The result is

$$\frac{\delta x_{max}}{R_p z_0} = \frac{1}{2}\sum_n D_n = 0.185. \qquad (31)$$

We have run a series of TWOQUICK simulations to test this analytic theory. The results are shown in Fig. 24

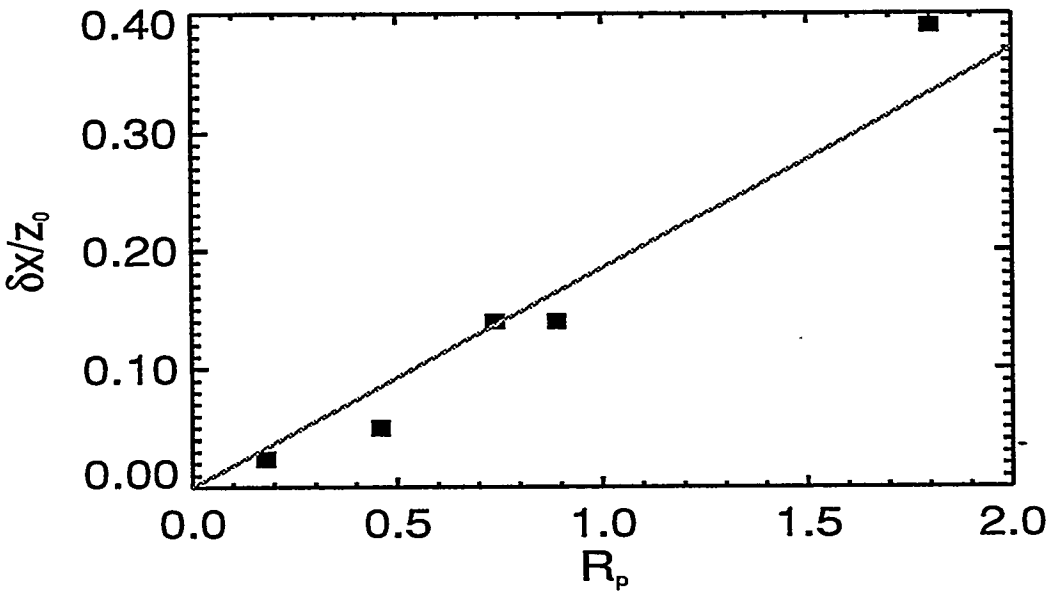

Fig. 24 TWOQUICK simulation points (squares) are compared to theory (line)

We can define the normalized shape function

$$X\left(\frac{z}{z_0}, \frac{x_0}{z_0}, \frac{x_1}{z_0}\right) = \frac{\delta x}{\delta x_{max}} = -5.4\sum_n \frac{D_n \sinh\alpha_n x_0 \sinh\alpha_n (x_0 - x_1)}{\sinh\alpha_n x_1} \cos\alpha_n z. \qquad (32)$$

It is instructive to consider the situation where only one foil or grid is present at a distance x_f from the virtual-cathode. Assuming an upstream foil we set x_f=x_0 and let x_1 go to infinity, for a down-stream foil, we set x_f=x_1-x_0 and let x_0 go to infinity. The shape of the virtual-cathode is the same in either case and is plotted in Fig. 25.

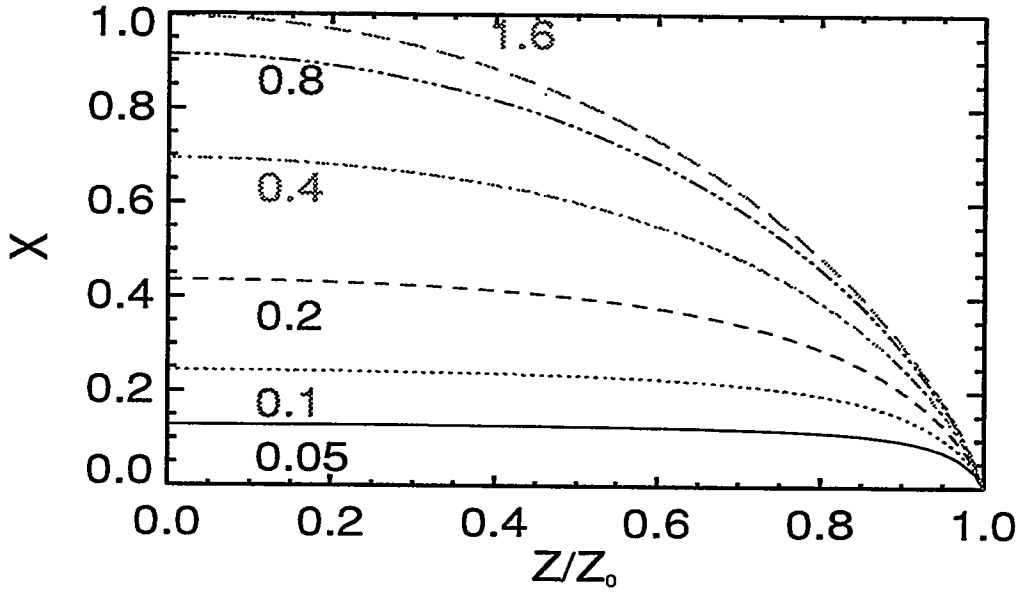

Fig. 25 The virtual-cathode shape curves are labelled with the value of x_f/z_0.

The flattening of the virtual-cathode for small x_f is clearly evident. This is due to the magnetic field pressure against the foil. It is also clear from the figure that when $x_f/z_0>1.6$ there is no change in the shape of the virtual-cathode. This is because the force imparted on the ion beam is distributed onto the wall ($z=z_0$). The magnitude of this force decays roughly exponentially with distance from the virtual-cathode. The scale length is approximately z_0 and thus placing a surface at a distance greater than z_0 from the virtual-cathode will have little effect.

C. Summary

The results can be summarized by the formula

$$R_{ef} \cong \frac{2.7 z_0}{R_p} \sqrt{1 + \frac{V_1}{V_2}}, \tag{33}$$

where R_{ef} is the effective focal length of the beam after acceleration through the gap with a curved virtual-cathode, $2z_0$ is the thickness of the beam in the direction of the applied magnetic field, V_1 is the kinetic energy of the ion coming into the acceleration stage, V_2 is the voltage across the gap, and R_p is the ratio of the beam induced pressure to the magnetic field pressure given by the formula

$$R_p = \frac{2\mu_0 J}{B_0^2}\sqrt{\frac{2M}{Q}}[\sqrt{V_1+V_2}-\sqrt{V_1}], \tag{34}$$

where J is the ion beam current density, B_0 is the applied magnetic field, M/Q is the charge-to-mass ratio of the ion.

VI. Multicusp accelerator

A. Emittance growth

The solenoidal focussing force acts as an effective transverse potential well given by the expression

$$\Phi_B = \frac{qB^2r^2}{4M}. \tag{35}$$

The potential due to the space-charge of the ions can be found from Poisson's equation

$$\nabla^2\Phi_{SC} = \frac{\rho}{\varepsilon_0}(1-f), \tag{36}$$

where we shall assume that f=0 for $r < r_i$ and is f_0 for $r > r_i$, where r_i is the minimum radius of the magnetic flux surface that intersects the cathode at the acceleration gap. Since the electrons are tied to the magnetic field lines, this is also the minimum radius that electrons can space-charge neutralize the beam. In section II we estimated the distance that ions will travel before they obtain a random transverse energy spread. Once this has occurred the beam density can be found from the Boltzmann relation

$$\rho = \rho_0 e^{-\frac{e\Phi}{kT}}, \tag{37}$$

where ρ_0 is the beam density at the center of the beam and $\Phi = \Phi_{sc} + \Phi_B$.

We solved these equations numerically and found that solutions only exist above a minimum beam temperature, T_{min}. The results can be expressed in terms of two dimensionless variables $\Gamma = \frac{\rho_0}{\rho_v}$ and

$$\Theta = \frac{4kT_{min}\varepsilon_0}{\rho_v eZr_i^2}, \tag{38}$$

where $\rho_v = \frac{\varepsilon_0 eZB^2}{M}$ is the beam density that would be balanced against the inward magnetic force. The parameter Θ is plotted as a function of Γ in Fig. 26. The ion divergence can be obtained from Eq. (38), the magnetic insulation condition eq. (2), and the relation $(\Delta\theta)^2 = \frac{kT_{min}}{Mv_B^2}$, where v_B is the beam final velocity. The result is

$$\Delta\theta = \frac{eZ}{v_B M}\sqrt{\frac{\Theta B V_c r_b}{2c}}, \tag{39}$$

were V_c is the critical insulating voltage of the accelerating gap and r_b is the outer radius of the ion beam. The beam emittance is obtained by multiplying eq (39) by r_b.

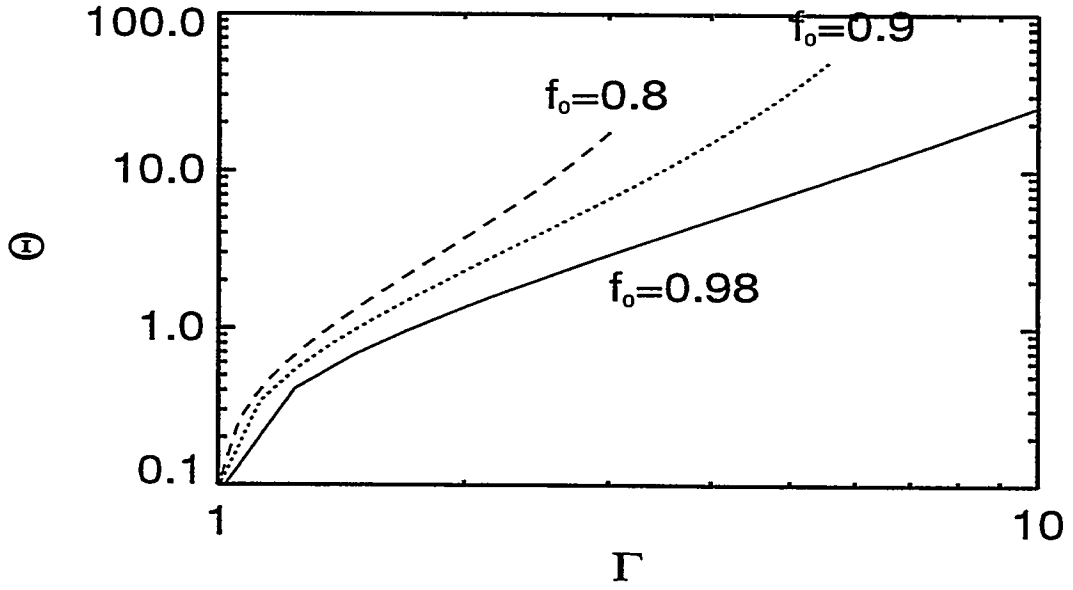

Fig. 26 The dimensionless parameter Θ is plotted as a function of the dimensionless parameter Γ.

Low divergence can be obtained by keeping the beam density in the unneutralized region as close to ρ_v as possible, i.e. $\Gamma \approx 1$. In practice, Γ will always be somewhat larger than 1,

because of aperture focussing at the acceleration gaps. Thus we can expect Θ to be of order unity.

B. Feasibility as a fusion driver

The beam requirements to drive inertial confinement fusion (ICF) capsules are extremely challenging. Numerical design calculations[14] of ICF capsule performance indicate optimal beam coupling is obtained for ions with a range of approximately 20mg/cm^2 in gold. This corresponds to a velocity of roughly 0.15c. A total beam power, P_T=700 TW is needed on a capsule with a radius, r_T, of 1 cm. The final focus, L_F, of the beam must be at least 2 m from the capsule to ensure survival of the hardware. Therefore, the beam divergence given by $\Delta\theta = \frac{r_T}{L_F}$, must be less than 5 mrad. This requirement could be relaxed if self-pinch transport works, allowing the focal length to be reduced to less than a meter. The beam brightness represents an overall figure of merit, which we can use to determine the feasibility of the multicusp accelerator approach. The field coils and support hardware for the final focussing magnets will reduce the total area that can be occupied by the beam. We estimate that the total beam area at the focussing element is given by $N_b \pi r_b^2 = \pi L_f^2$, where N_b is the number of beams. Therefore, the beam brightness required for ICF is

$$B_{BF} = \frac{P_T}{\pi r_T^2} = 2.2\text{x}10^{18}\ \text{W/m}^2. \tag{40}$$

The maximum beam brightness that can be achieved with the multicusp accelerator approach can be determined from the relation

$$B_B = \frac{F_B J V_F}{(\Delta\theta)^2} \tag{41}$$

where F_B is the beam bunching factor, and V_F is the final voltage of the ions. Using eqs (3) and (39) we obtain

$$B_B = \frac{F_B \varepsilon_0 B c^4 M \beta^3 N_S \sqrt{N_B}}{(1-f) q L_F \Theta}, \tag{42}$$

where N_S is the number of acceleration stages. Setting $B_B > B_{BF}$, we obtain the condition

$$N_s > \frac{3.0 \times 10^3 (1-f) L_F \Theta}{\beta^3 A F_B B \sqrt{N_B}}. \tag{43}$$

The physics behind this result is that increasing the number of acceleration stages decreases the voltage on each acceleration stage, thus V_c is smaller and so is r_i, reducing the transverse potential at the center of the annular beam. The number of stages N_s=100 for the set of parameters, e.g. A=39, f=0.9, L_F=2m, Θ=1.0, F_B=2, B=5, N_B=20, and β=0.15. Assuming that the final beam energy is 400 MeV, each stage will have 4 MV applied to it. The over all length of the accelerator would be determined by the inductive core material and should be about 200 m, which is considerably shorter than a conventional heavy ion accelerator. However, in section II we showed that a high degree of neutralization (better than 95%) would be required if the accelerator is longer than about 125 m. Therefore, the lack of space-charge neutralization at the center of the beam does not strictly rule out the potential advantages of this accelerator concept as a driver of ICF, but high degrees of charge neutralization will be required. The only approach that seems feasible is to use plasma injection.

There are other important issues, which must be studied to determine the feasibility of the multicusp approach. One issue is the aperture focussing at each acceleration stage. This focussing can be significantly stronger in the multicusp accelerator than in a conventional linac, because of the formation of a virtual cathode on the down-stream side of the acceleration gap. Another issue is the accuracy that the focussing forces can be balanced against the outward space-charge forces, since the net imbalance will create beam emittance. This has been studied by numerical simulation. An example simulation is described in the next section.

VII. Multicusp accelerator simulations

We used the code TWOQUICK to study the multicusp accelerator concept. The injection stage is critical to the success of any multistage accelerator. A geometry and applied magnetic field (B=10 Tesla) of a cusp insulated injector is shown in Fig. 27.

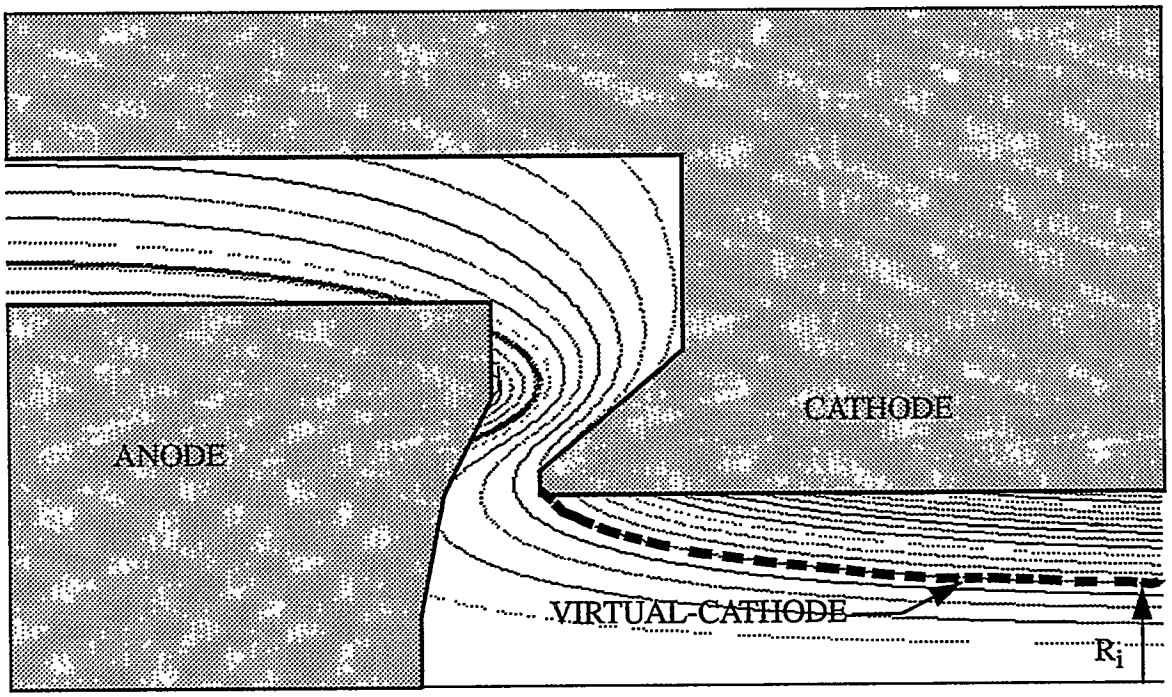

Fig. 27 An injector insulated by a cusp magnetic field

The main challenge of designing the injector is to determine the correct shape of the anode emitting surface. The object is get the beam to enter the virtual-cathode with no radial component to the velocity. Since the beam is not space-charge neutralized until it crosses the virtual-cathode there will be an outward force. Thus the beam must be given a small inward radial velocity component by slanting the anode emitting surface as shown schematically in Fig. 27. TWOQUICK can only a generate rectangular mesh in the r-z plane, but it is capable of emission off of diagonals across this mesh. Still this is not enough freedom to accurately determine the shape of the anode surface so that ions entering the virtual-cathode will have no radial motion. We were able to get an approximate shape and it

appears that given a code with boundary fitted coordinates, a suitable injector could be designed. The radial ion density profile must also be suitable. The desired current profile is roughly a step function at r_i, $J=J_{sx}$ [eq (3)] with f=0 for $r < r_i$ and f determine by effectiveness of the neutralization process for $r > r_i$. We assumed 30 MV of acceleration per stage in spite of the results of the last section to get the final energy up closer to that of a fusion driver. Assuming singly charged potassium ions and f=0, Jsx=1.4 A/cm^2. The ion current density will depend on the effective accelerating gap. Some insight into this dependence can be gained by considering the Child-Langmuir equation

$$J_{CL} = \frac{4}{9}\varepsilon_0\sqrt{\frac{2q}{M}}\frac{V^{3/2}}{d^2}, \tag{44}$$

which is the one dimensional space-charge-limited current. The gap between the anode and the virtual-cathode is a monotonically decreasing function of radius and thus injector will generate an ion current density profile that increases with radius. The effective gap for $r < r_i$ should be approximately 30 cm for our case. If we assume that 100 A/cm^2 can be neutralized for $r > r_i$ (98.6% neutralized) the effective gap must be about 3.5 cm. This is a rather large variation in the accelerating gap. The low current densities required for $r < r_i$ could be attained by recessing the central portion or by providing an ion source over only a fraction of the available area.

Beam propagation after the injector depends of the balance of the radial forces averaged over the ion trajectories. We separated the difficulties of designing the injector from subsequent beam propagation by numerically injecting a perfectly laminar beam into the simulations, with a spin consistent with the axial magnetic field. The injected beam current density was set by eq. (3) with f=0 for $r < r_i$. Various current densities were tried for $r > r_i$, Typically using too large a beam current density resulted in the beam expanding into the drift tube walls. The inward forces consist of the solenoidal force already considered and electrostatic forces at the acceleration gaps (aperture focussing). Equipotential surfaces within the gap can be found from the equation

$$jx^2 = [\sqrt{1+w-\psi} - \sqrt{w}][\sqrt{1+w-\psi} + 2\sqrt{w}]^2, \quad (45)$$

were w is the ion energy normalized to the gap voltage, Ψ is the potential normalized to the diode gap, $x=d/d_0$ where d_0 is the gap determine by the Child-Langmuir equation, and $j = \frac{16J}{9J_{CL}}$. Equation (41) can be used to determine the appropriate accelerating gap be setting $\Psi = 0$. This sets the E=0 surface at anode and minimizes curvature of the equipotential surfaces. Maintaining this condition requires that the acceleration gaps increase with distance down the accelerator as seen from the following table

w	J/J_{cl}	d/d_0
0	1.0	1.0
1	2.2	1.5
2	2.6	1.6
4	3.0	1.7
8	3.6	1.9
12	4.0	2.0

Slanting the electrodes that feed power into the gap in a manor analogous to Pierce electrodes can be used to counter the outward space-charge of a finite beam. The appropriate shape can be found from eq. (45) by analytic continuation off the real axis. The resulting shapes are shown in Fig. 28. Increasing/decreasing the slant of these feeds beyond that calculated results in a net inward/outward force at each gap. This is one degree of freedom that can be used to balance the radial forces on the beam.

Previous simulations have indicated that passive neutralization of the ion beam is not adequate, because the accelerating electric field pulls more electrons into the beam near r_i than at larger radii. This effect can be reduced by injecting plasma in the region just down stream of each accelerating gap.

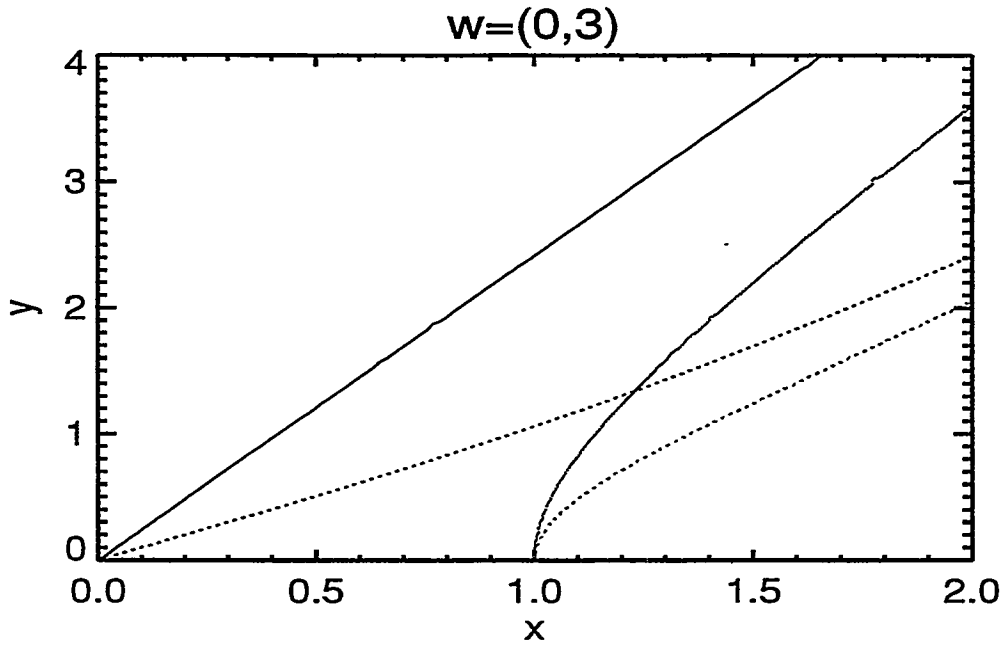

Fig. 28 Generalized Pierce electrode shapes

A snap shot of a simulation of five stages of acceleration using all of these consideration is shown in Fig. 29. The beam in injected from the left side. The injected current density is 100 A/cm^2 for $r > r_i = 9$ cm. The current density is 1.4 A/cm^2 for $r < r_i$. Nearly 100% of the beam exits the simulation on the right hand side. However, a real accelerator would have to be considerably longer than this simulation, due to the requirement that each acceleration stage be inductively isolated from the next. A longer accelerator would require a more accurate balance between the inward focussing force and the outward force due to the net beam space-charge. The radial divergence of the ion beam was approximately 30 mrad at the end of the simulation. Clearly low emittance and intense focussing will be difficult to achieve with the multicusp accelerator configuration. The generation of neutrons may be a promising application for this type of accelerator, since a very high quality beam is not required. Furthermore, protons can be used to generate neutrons and from eq (3) we see that solenoidal transport is well suited to low mass ions

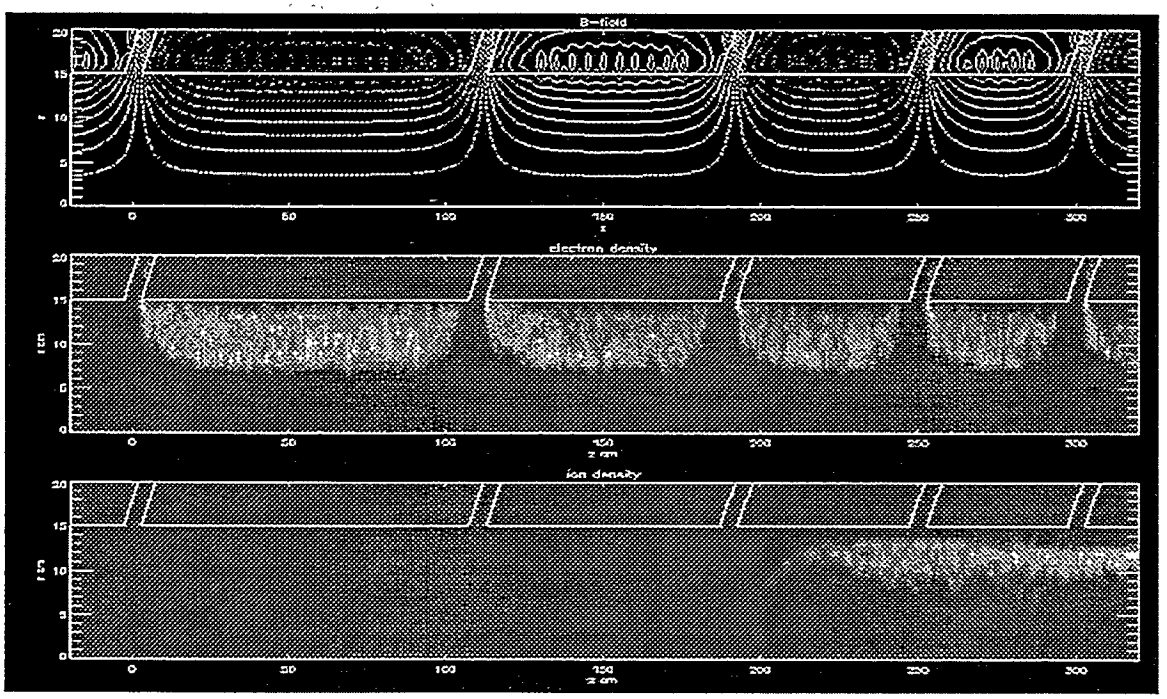

Fig. 29 The magnetic field, electron density, and ion density of a simulation of five stages of a multicusp accelerator

VIII. Conclusions

We have studied the possibility of using space-charge neutralization to increase the current that can be transported in an ion induction linac. We have presented 3-D PIC simulations of ion beams neutralized by electrons emitted from the drift tube walls. The neutralization factor was approximately 96% when no magnetic field was present. However, the acceleration gaps must be magnetically insulated due to the presence of electrons. We found that a field of only 1 Tesla normal to the surface reduced the neutralization factor to approximately 80%. This explains the poor transport that was observed in the return flux region of the pulselac experiments that used a radial magnetic field to insulate the acceleration gaps. We have presented analytic calculations and numerical simulations of the space-charge neutralization of an ion beam by a preformed plasma, which indicate that a plasma injected into the return flux region could remove this problem. We tested plasma injection experimentally using the ALIAS facility and found a significant reduction in the

beam space-charge. However, the radial field geometry requires field coils inside of the beam and support structure for these coils. These supports will be struck by the beam and cause out-gassing of material that can cause stripping of the beam ions. Furthermore, the support structures will be eroded, which posed some practical difficulties for a reactor scenario. Perhaps these difficulties can be overcome by some kind of beam divertor to keep ions from striking the support structures. Another approach is to only use field coils outside of the beam. This will set up a cusp magnetic field. We performed 3-D PIC simulations of a beam injected across acceleration gaps insulated by such a cusp field. We found that electrons leaving the drift tube walls effectively neutralized an annular region of the beam, but the electrons were tied to field lines and could not neutralize the central portion of the beam. We then developed a simple model of the beam emittance induced by the nonneutralized portion of the beam. The model indicates that a large number of stages are required for a multicusp accelerator to generate a beam brightness sufficient to drive fusion. We performed 2-D PIC simulations of a multicusp accelerator. The beam emittance is determine by the degree of balance between the focussing forces and the net space-charge forces. The divergence of the beam at the end of six stages of acceleration (180 MeV potassium) was approximately 30 mrad, which is too large to focus on a fusion capsule. It is not clear how small the divergence could be made with careful design. We believe that the multicusp accelerator is better to suited to applications that do not require low beam divergence such as generating neutrons by accelerating protons, which are strongly focussed by the solenoidal field.

We developed general arguments that suggest that a space-charge neutralized light to medium mass ion accelerator using just a few stages and relatively short overall length will probably have the best chance of producing the beam quality needed to drive fusion targets. The radial field geometry is probably most suited to this type of acceleration scheme if the issue of the support structures can be solved.

References

1 P. Dreike, C. Eichenberger, S. Humphries, Jr., and R. N. Sudan, J. Appl. Phys. **47**, 85 (1976); S. Humphries, Jr., R. N. Sudan, and L. Wiley, J. Appl. Phys. **47**, 2382 (1976).

2 S. Humphries, Jr. J. Appl. Phys. 49, 501 (1978).

3 D. J. Johnson and T. R. Lockner, J. Appl. Phys. 61, 20 (1987).

4 S. Humphries and J. Poukey, Particle Accelerators, 10, 107 (1980).

5 O. Batishchev, V. Golota, V. Karas, V. Kiyashko, E. Kornilov, Y. Sigov, I. Silaev, and Y. Fainberg, Plasma Phys. Rep. 19, 313, (1993).

6 E. Stuhlinger, *Ion Propulsion for Space Flight*, (McGraw-Hill, New York, 1964), p. 232.

7 D. B. Seidel, M. L. Kiefer, R. S. Coats, A. L. Siegel, and J. P. Quintenz, "QUICKSILVER-A 3-D, electromagnetic, PIC code," in Proc. 12th Conf. Numerical Simulation of Plasmas, San Francisco, CA, paper PT_24, 1987.

8 D. B. Seidel, M. L. Kiefer, R. S. Coats, T. D. Pointon, J. P. Quintenz, and W. A. Johnson, in *Computational Physics*, edited by A. Tenner (World Scientific, Singapore, 1991), pp. 475-482.

9 J. P. Quintenz and D. B. Seidel, M. L. Kiefer, T. D. Pointon, R. S. Coats, S. E. Rosenthal, T. A. Mehlhorn, M. P. Desjarlais, and N. A. Krall, Laser and Particle Beams, 283, (1994).

10 T. D. Pointon, M. P. Desjarlais, D. B. Seidel, S. A. Slutz, R. S. Coats, M. L. Kiefer, Phys. Plasmas, 1, 429, (1994).

11 W. Lotz, Zeitschrift fur Physik, 216, 241 (1968).

12 Eugene J. McGuire, Lasers and Particle Beams, 13, 321, (1995).

13 D. J. Johnson, S. R. Kurtz, and M. A. Sweeney, J. Appl. Phys., 61, 5314, (1987).

14. R. E. Olson, G. O. Allshouse, D. L. Cook, T. R. Lockner, M. G. Mazarakis, C. L. Olson, D. L. Smith, in: 15th IEEE/NPSS Symposium on Fusion Engineering Vol I, p. 189, 1993,(IEEE catalog number 93CH3348-0)

distribution

4 Cornell University
Laboratory of Plasma Studies
Attn: R.N. Sudan
D. A. Hammer
J. B. Greenly
B. R. Kusse
369 Upson Hall
Ithaca, NY 14853

2 Gesellschaft fuer Schwerionenforschung
Attn: Rudolf Bock
Ingo Hofmann
P. O. Box 110552
D-64220 Darmstadt, Germany

1 I.N.R., Forschungzentrumkarlsruhe
Attn: Hans Bluhm
Postfasche 3640
D-76021, Karlsruhe, Germany

3 Lawrence Berkeley National Laboratory
Attn: R. O. Bangerter
E. P. Lee
A. Faltens
1 Cyclotron Rd
Berkeley, CA 94720

2 Lawrence Livermore National Laboratory
Attn: A. Friedman L-440
B. G. Logan L-481
P.O. Box 5511
7000 East Ave
Livermore, CA 94550

2 Naval Research Laboratory code 6771
Attn: P. F. Ottinger
F. C. Young
Washington, DC 20375

1 Universitaet Erlangen
Attn: D. H. H. Hoffmann
Erwin-Rommel-Str. 1
91058 Erlangen, Germany

1 Stanford Linear Accelerator Center
Attn: W. B. Herrnannsfeldt
P. O. Box 4349
Stanford, CA 94309

1	QM Technologies Attn: T.R. Lockner 3701 Howkins St. NE Albuquerque, NM 87109		
1	S. Humphries, Jr 13407 Sunset Canyon Dr. NE Albuquerque, NM 87111		
1	MS-0188	4523	C.E. Meyers
1	MS-0151	9000	G. Yonas
1	MS-1186	9541	C. Olson
10	MS-1186	9541	S. A. Slutz
1	MS-1186	9541	M. P. Desjarlais
1	MS-1186	9541	J. Poukey
1	MS-1186	9541	M. Sweeney
1	MS-1187	9533	T. A. Mehlhorn
1	MS-1187	9533	A. Filuk
1	MS-1187	9571	K. Matzen
1	MS-1187	9571	E. McGuire
1	MS-1190	9500	D. L. Cook
1	MS-1193	9531	J. E. Maenchen
1	MS-1193	9531	M. Cuneo
1	MS-1193	9531	D. J. Johnson
1	MS-1193	9531	M. Mazarakis
1	MS-1193	9531	P. Primm
1	MS-1193	9531	T. Renk
1	MS-1195	9502	J. P. Quintenz
1	MS-1196	9577	R. Leeper
1	MS-1196	9577	J. Bailey
1	MS-9018	8940-2	Central Technical Files
5	MS-0899	4414	Technical Library
2	MS-0619	12690	Review and Approval Desk For DOE/OSTI